Int J Earth Sci (Geol Rundsch) (2006) 95:587–607
DOI 10.1007/s00531-006-0090-x

ORIGINAL PAPER

Hybridization of mafic microgranular enclaves: mineral and whole-rock chemistry evidence from the Karamadazı Granitoid, Central Turkey

Kerim Kocak

Received: 11 April 2005 / Accepted: 3 February 2006 / Published online: 11 May 2006

Abstract On the Eastern Tauride Belt, the Cretaceous calc-alkaline Karamadazı Granitoid consists of quartz diorite containing mafic microgranular enclaves (MME) and leucocratic granite. The quartz diorite consists of plagioclase (An_{8-65}), hornblende, biotite, K-feldspar, quartz, epidote and titanite. Subrounded MME in the quartz diorite are holocrystalline, fine-grained, quartz diorite to diorite in composition, and display a similar mineral assemblage to their host. Large crystals in MME and quartz diorite show various disequilibrium microstructures indicative of hybridization. Plagioclase crystals exhibit inverse, normal, and oscillatory zoning with maximum core-to-rim An content increase up to 38% in the enclave and 40% in the quartz diorite. Both hornblende and augite exhibit normal and reverse zoning even in the same sample. The new field, textural, mineral compositional, and geochemical evidence leads to the conclusion that MME could have formed through injection of successive pulses of basic magma into upward mobile magma chambers containing cooler, partially crystalline quartz diorite magma. The quartz diorites show similarity to high-Al TTG (tonalites–trondhjemites–granodiorites), with their high Na_2O, Sr, LREE, and low Mg#, Cr, HREE contents, and are suggested to be produced by extensive interaction between the crustal and mantle-derived melts through mixing at depth. In contrast, leucogranites have geochemical characteristics distinct from the quartz diorites and MME, and are probably not involved in MME genesis.

Keywords Granite · Enclave · Mixing/Mingling · Geochemistry · Turkey

K. Kocak (✉)
Department of Geological Engineering,
Selcuk University, 42075 Konya, Turkey
e-mail: kkocak@yahoo.com

Introduction

Mafic microgranular enclaves (MME) play a substantial role in the evolution of granitic magmas, and have been studied by many authors (e.g., Didier 1973; Chappell et al. 1987; Chen et al. 1989; Dodge and Kistler 1990; Didier and Barbarin 1991; Barbarin and Didier 1992; Elburg 1996; Maas et al. 1997). Of all the enclave varieties present in granitic rocks, MME have been the most controversial and the subject of several detailed studies (e.g., Frost and Mahood 1987; Didier and Barbarin 1991; Michael 1991; Blundy and Sparks 1992; Silva et al. 2000; Barbarin 2005). They occur as fragments of fine-grained igneous rocks, generally with ovoid shape and sharp contacts, representing blobs of coeval magmas (Didier and Barbarin 1991), and characterized by distinctive microstructures commonly interpreted as igneous in origin (e.g., Vernon 1990). 'Mafic' indicates that these enclaves are darker-colored than their enclosing granitoid (Barbarin 2005). Petrogenetic hypotheses for the origin of MME fall into three main categories: (1) settling of early crystals from the host magma or by fragmentation of early solidified wall-rock facies closely related to the host magma (e.g., Dodge and Kistler 1990; Dahlquist 2002); (2) globules of a more mafic, generally hybrid

magma, co-mingled with more felsic host magma (e.g., Didier 1973; Vernon 1983, 1990; Holden et al. 1987); (3) fragments of recrystallized, refractory metamorphic rocks and fragments of melt residues from the granite source (Chappell et al. 1987; Chen et al. 1989; White et al. 1999).

Previous studies of the felsic-mafic Karamadazı Granitoid reported magma mingling had occurred (e.g., Kuscu et al. 2001; Boztug et al. 2002), but neither mineral chemistry nor whole-rock geochemistry of the enclave had been investigated. The objective of this present study is to investigate the microstructures, mineral and whole-rock chemistry of the Karamadazı Granitoid to determine the origin of the hybridization process and its petrological implications.

Geological setting and field characteristics

Turkey is an essential component of the Alpine–Himalayan orogenic system. It includes a number of continental blocks separated by suture zones, formed by the closure of the different branches of the Neo-Tethyan ocean during the late Cretaceous–Eocene (Şengör and Yilmaz 1981) (Fig. 1a).

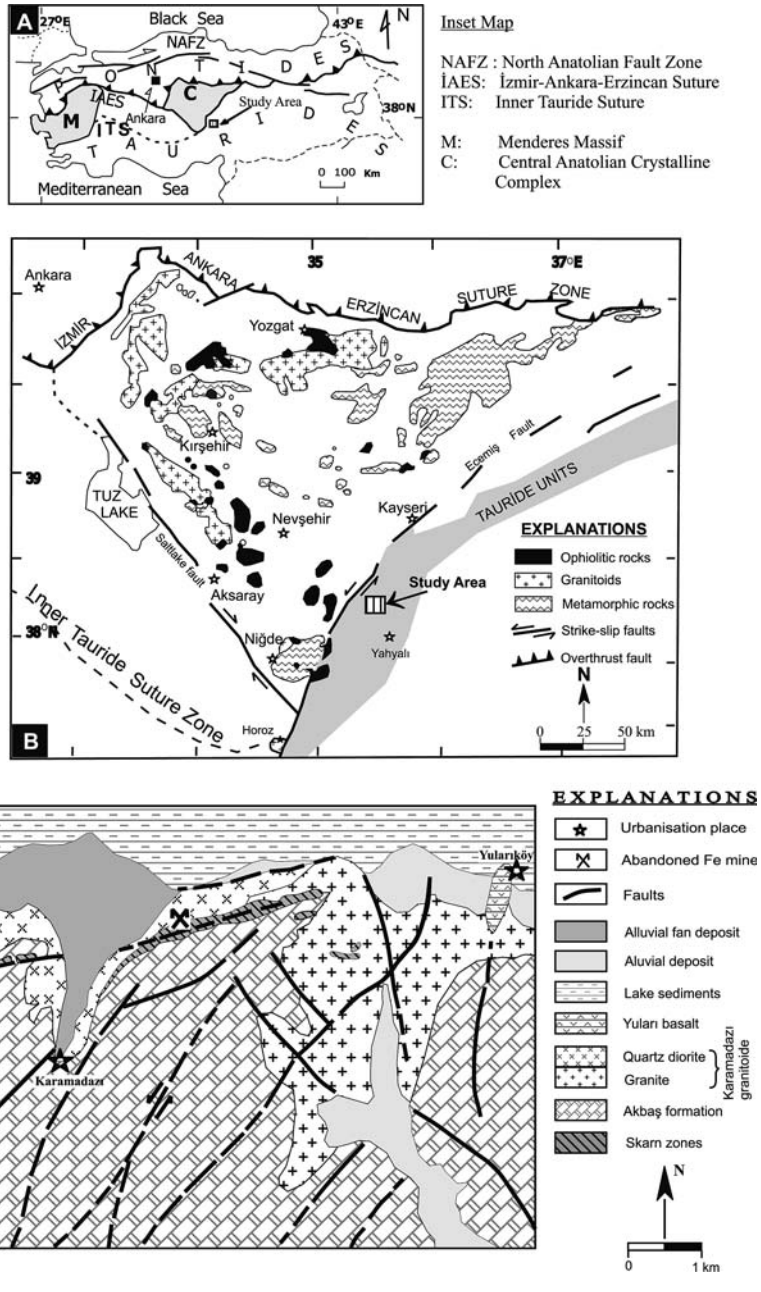

Fig. 1 Simplified location map (**a**) and geological map (**b**) of the Central Anatolian Crystalline Complex, and geological map (**c**) of the Karamadazı area (Kuscu et al. 2001)

The intrusion of granitic plutons along the northern edge of the Taurides, Central Turkey, is attributed to the closure of the ''Inner Tauride Oceanic domain'' (Gorur et al. 1984; Dilek et al. 1999), a branch of Neo-Tethys. Two subduction zones with opposite vergence are invoked to account for a double granitic arc, in the North (Central Anatolian Crystalline Complex; Goncuoglu et al. 1991) and in the South (northern edge of the Menderes-Tauride platform).

In the northern Taurides, granitic magmatism is represented by the Karamadazı Granitoid (Gorur et al. 1998; Kuscu et al. 2001), located about 40 km South of the locality of Kayseri, and by the Horoz granodiorite (Fig. 1b). Both granitoids are considered to be cogenetic with similar granitoids from Central Anatolia (Goncuoglu et al. 1993; Kuscu et al. 2001), whose tectonic settings are suggested as collisional/post-collisional (Goncuoglu and Tureli 1994; Akiman et al. 1993; Erler and Goncuoglu 1996; Boztug 1998, 2000; Aydin et al. 1998; Yaliniz et al. 1999) and/or magmatic arc (Gorur et al. 1984; Kocak 1993; Kocak and Leake 1994; Kadioglu and Gulec 1996).

The Karamadazı Granitoid was reported as being zoned from East to West, from granite and granodiorite, to quartz diorite with MME (Oygur et al. 1978; Oygur 1986). Such a regional zoning is not confirmed in the field. The Karamadazı Granitoid can be separated into only two main units: quartz diorite with MME to the west, and felsic granite to the east (Fig. 1c; Kuscu et al. 2001). The granitoid intruded into the Akbas Formation, a series of low-grade metamorphic carbonates and orthoquartzite lenses, inducing development of a skarn zone with iron ore. Skarnization process induced alteration of plagioclases and mafic minerals mainly to epidote and widespread silicification in skarnized plutonic rocks. The leucocratic granites have mostly concordant contacts with country rocks, whereas aplite and pegmatite dikes cut through the granites.

An open pit, iron mine at the center of the Karamadazı Granitoid (Fig. 1c) presents excellent exposure to study the hybridization of mafic microgranular MME. Rounded MME are mostly 15–120 mm in diameter (Fig. 2a), but range from a few millimeters to 0.5 m in size. MME usually display a fine-grained margin against the host rock (Fig. 2a, d). Locally, some felsic haloes develop in the granitoid hosts near the contact with the enclaves (Fig. 2b), indicating an interaction between mafic (enclave) and surrounding felsic (granitic) magma. The geometry of the enclave–host contact changes from sharp/crenulate to diffuse/veined over a distance of a few centimeters. Smaller MME tend to be finer grained and more isotropic than larger ones. The disaggregation of some MME yields heterogeneous hybrid rocks containing wispy schlieren and clots of fine-grained mafic material (Fig. 2c, d). Locally, MME are highly concentrated (clusters, >30% of the whole rock) and in such cases, the matrix typically shows irregular leucocratic patches (Fig. 2d).

Petrography and mineral chemistry

Methods

Fifty petrographic thin sections were examined under the microscope to determine composition and texture,

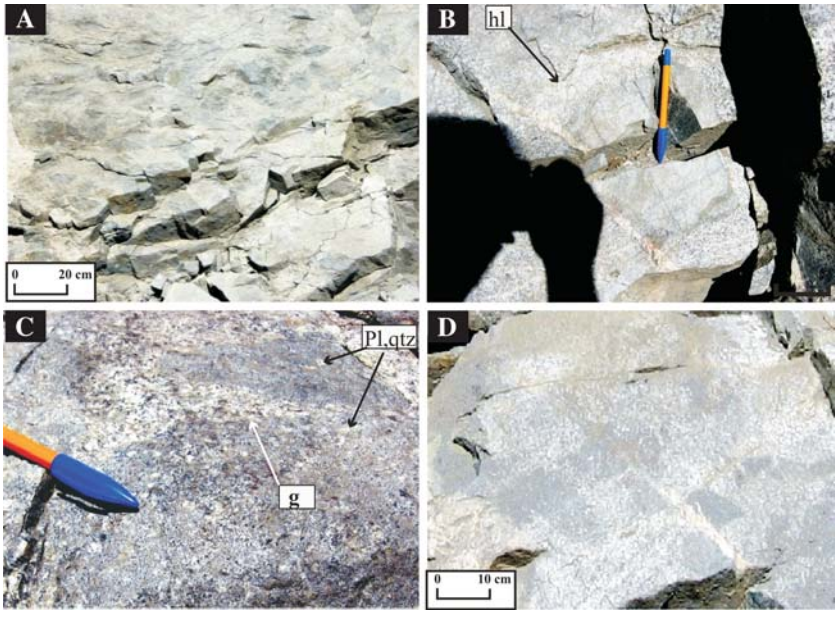

Fig. 2 Field photographs showing **a** small mafic microgranular enclaves; **b** the development of felsic haloes (*hl*) between the granitoid hosts and enclaves; **c** wispy schlieren in quartz diorites, and mafic microgranular enclaves (*MME*) with gradational contact (*g*). Plagioclase (*pl*) and quartz (*qtz*) crystals moved into MME; **d** heterogeneously distributed enclaves in the intermediate rocks. Small pen represents ~12 cm

16 of which were analyzed by point counting. Polished sections (25 × 46 mm) of representative rock samples were made at the thin-section Laboratory of Geological Engineering Department, Karadeniz Technical University (Trabzon). Polished slides were coated with carbon and then analyzed at the Electron Microprobe Laboratory of McGill University, Montreal, Québec, Canada. Mineral analyses were carried out on a JEOL JSM35 Electron Microprobe running Link QX2000 energy dispersive analytical software. Electron beam condition was 15 keV and 15 nA. Fe^{3+} contents in amphiboles and pyroxenes were calculated according to Droop (1987).

General petrography

Quartz diorites (Fig. 3) consist of plagioclase (45–65 vol%), hornblende (13–35%), biotite (2–12%), K-feldspar (1–20%), quartz (3–21%), and accessory epidote, titanite, magnetite, calcite and apatite (Table 1). MME are holocrystalline and have the same mineral assemblage as their quartz diorite host. MME consist of plagioclase (40–62%), hornblende (20–36%), biotite (1–15%), K-feldspar (0–15%), clinopyroxene (0–15%), quartz (0–15%), and accessory epidote, titanite, magnetite, calcite and apatite. MME are equigranular, fine-grained (Fig. 4a, b) and occasionally porphyritic.

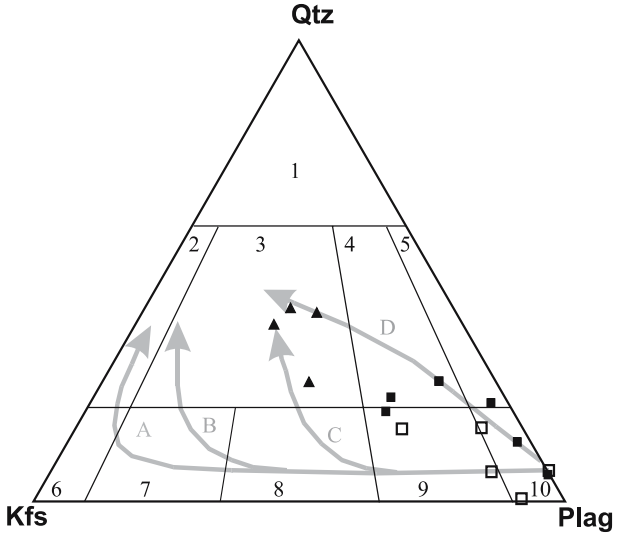

Fig. 3 Modal compositions in a Qtz–Kfs–Plag ternary diagram: granites (*filled triangles*), enclaves (*open square*), quartz diorites (*filled square*). Simplified fields of plutonic rocks after Le Maitre et al. (1989): *1* quartz-rich granitoid, *2* alkali feldspar granite, *3* granite, *4* granodiorite, *5* tonalite, *6* alkali feldspar syenite, *7* syenite, *8* monzonite, *9* monzodiorite/monzogabbro, *10* diorite–gabbro. Main trends of plutonic rocks series (*grey arrows*) after Lameyre and Bonin (1991): *A* strongly alkaline, *B* mildly alkaline, *C* monzonitic, *D* calc-alkaline

Poikilitic textures mostly show subhedral biotite and hornblende engulfed by plagioclase (Fig. 5a) or alkali feldspar. Titanites are mostly anhedral with interstitial habit in quartz diorite and MME, and appear to result from subsolidus recrystallization involving hornblende and biotite (Fig. 5b). Acicular apatite, 0.3 mm in maximum length, is a common feature of mafic melt globules trapped in silicic magma and often cited as evidence of quenching (Wyllie et al. 1962) (Fig. 5c). The increase of felsic mineral components, generally as megacrysts and leading to lighter colors, is inferred to reflect the intensity of hybridization. Interaction between mafic (enclave) and surrounding felsic (granitic) magma is clearly viewed in the host rocks between close MME, where amphibole crystals develop so as to define linear fabric. The leucogranites are made up of medium-coarse grained plagioclase (23–34%), K-feldspar (22–32%), quartz (23–38%), biotite (1–12%), ± actinolitic hornblende (0–8%) with accessory apatite, titanite, zircon, and allanite.

Plagioclase

In the quartz diorites, plagioclase occurs both as large euhedral crystals (up to 6 × 2.5 mm) and as small subhedral crystals (≈ 0.6 × 0.6 mm). Compositions range from An_{31} to An_{65} in the cores to An_{8} to An_{34} in the rims (Table 2; Fig. 6). Both plagioclase types exhibit normal, inverse or oscillatory zoning (Figs. 7, 8) and embayment. This is commonly interpreted as resulting from magma mingling in silicic-intermediate rocks (Stamatelopoulou-Seymour et al. 1990; Stimac and Pearce 1992). The large euhedral grains are not abundant but are homogeneously distributed in the rock. These grains form laths with an aspect ratio ca. 1:1.5 and commonly host inclusions of subhedral biotite and anhedral, brown hornblendes. In the MME, plagioclase crystals are smaller or of equal size than those in the host granite. Their composition ranges from An_{32}–An_{66} in the cores to An_{20}–An_{55} in the rims (Table 3), which indicates that the rims of plagioclase in MME are notably more calcic than the ones in the host. In both rock types, plagioclase sporadically forms rims around hornblende grains. Compositional dissimilarities of plagioclase phenocrysts in quartz diorite to those of enclave imply that MME were mostly not equilibrated with their hosts.

Hornblende

Hornblende in quartz diorite samples often shows conversion to the brown biotite along its cleavage, and forms both phenocrysts (5.1 x 1.8 mm) and matrix

Table 1 Modal compositions (%) of the Karamadazı Granitoid (1,000 points are counted for each sample)

	Quartz diorite					Enclaves							Granite			
Sample no.	26	38	40	43	47	34e	36e	38e	40e	43e	44e	49e	57	60	62	65
Quartz	3.2	9.6	21.4	15.1	17.2	4.59	0.2	10.2	4.3	9.7	14.6	4.68	38.4	34.6	35.2	22.8
Orthoclase	0.9	2.5	9.3	19.9	3.3	0.1	5.0	5.1	0.0	14.6	0.0	8.64	28.7	32.3	22.4	31.7
Plagioclase	54.5	65.0	52.1	45.0	60.7	61.47	54.4	48.3	61.3	38.3	44.3	61.65	25.1	23.2	27.8	34.2
Biotite	2.0	11.7	3.5	3.2	3.8	8.9	1.7	14.8	9.1	9.7	3.2	1.42	6.7	7.3	11.9	1.2
Hornblende	35.0	9.9	13.1	15.0	13.7	22.4	28.6	19.7	24.1	25.8	35.8	18.7	0.0	0.0	0.0	8.1
Augite	0.0	0.0	0.0	0.0	0.0	0.0	6.1	0.0	0.0	0.0	0.0	3.2	0.0	0.0	0.0	0.0
Zircon	0.0	0.0	0.0	0.0	0.4	0.9	0.0	0.0	0.0	0.0	0.0	0.0	0.0	0.0	0.0	0.0
Magnetite	0.8	0.3	0.0	0.8	0.8	1.6	0.0	0.0	0.3	0.4	0.4	0.0	0.6	0.9	0.8	0.2
Epidote	1.9	0.0	0.3	0.2	0.0	0.0	1.2	0.0	0.0	0.0	1.1	1.2	0.0	0.0	0.0	0.0
Calcite	0.0	0.0	0.0	0.0	0.0	0.0	1.3	0.0	0.0	0.0	0.0	0.0	0.0	0.0	0.0	0.0
titanite	1.2	0.9	0.2	0.4	0.0	0.0	1.1	1.5	0.5	0.8	0.0	0.3	0.4	1.3	1.4	0.9
Apatite	0.4	0.0	0.0	0.3	0.0	0.0	0.3	0.3	0.3	0.6	0.5	0.2	0.0	0.3	0.4	0.4
Tourmaline	0.0	0.0	0.0	0.0	0.0	0.0	0.0	0.0	0.0	0.0	0.0	0.0	0.0	0.0	0.0	0.4
Total	99.9	99.9	99.9	99.9	99.9	99.9	99.9	99.9	99.9	99.9	99.9	99.9	99.9	99.9	99.9	99.9

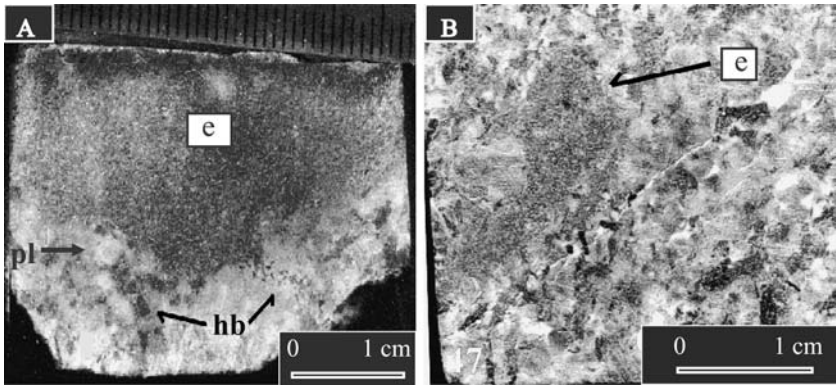

Fig. 4 Photos of **a** hornblende (*hb*) injected into quartz diorite and mafic microgranular enclaves (*MME*) (*e*). Plagioclase (*pl*) xenocrysts lay across the enclave contacts. **b** Small enclave, with composition close to its host rocks

crystals (2–0.8 mm). Hornblende in enclave samples also forms in two grain sizes: (a) coarse-grained (3 × 0.75 mm) and (b) fine-grained (0.3 × 0.18 mm). In general, both varieties of hornblende are subhedral, and it is common to observe assemblages with biotite, epidote, and titanite. The coarse-grained hornblende often shows transition to biotite along its cleavage (Fig. 5b), and is sometimes granulated along its edge, and enclosed by plagioclase. Remnants of clinopyroxene are commonly found in the core of poikilitic hornblendes.

In the IMA-approved nomenclature (Leake et al. 1997), hornblende is classified as predominantly magnesio-hornblende and minor actinolite (Fig. 9a). In comparison with hornblende of the host rock, hornblendes of MME are slightly richer in Si (Tables 4, 5), though they almost overlap on the classification diagram of Leake et al. (1997) (Fig. 9a). Hornblende phenocrysts show reverse zoning in terms of decreasing $Mg/(Mg + Fe^{2+})$, indicating disequilibrium crystallization with magma (Fig. 9b). Both reverse and normal zoning in the hornblendes of MME also exist in the same sample.

Pyroxene

Pyroxene is found only in enclave samples, and generally shows conversion to amphibole around its edges. Pyroxene is augite in composition (Table 6; Fig. 10), exhibiting normal and/or reverse chemical zonation, and can coexist with biotite in the same sample. The reverse zoning of pyroxene may indicate an open system behavior (Bloomfield and Arculus 1989). The clinopyroxene relicts engulfed by hornblende in the MME seems to reflect non-equilibrium conditions involving reaction of clinopyroxene with its surrounds.

Biotite

Biotite is observed both as phenocrysts with/without inclusions of hornblende or as inclusions within the hornblende and plagioclase. It is green and brown in

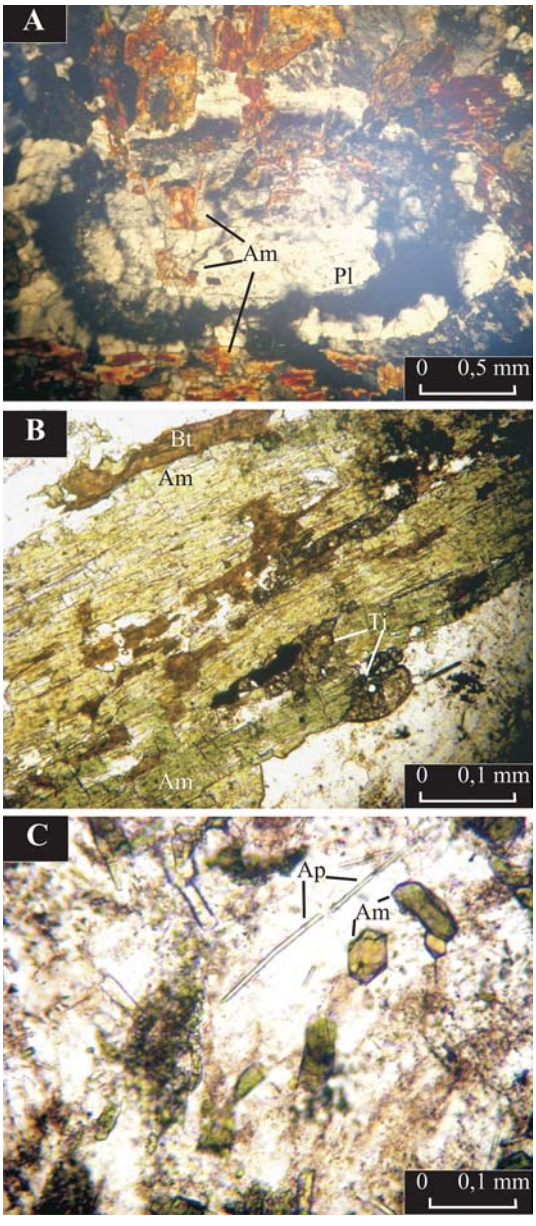

Fig. 5 Plane-polarized light photomicrographs of typical minerals located in the mafic microgranular enclaves (*MME*); **a** poikilitic plagioclase (*pl*) with hornblende (am) inclusions; **b** anhedral titanite (*ti*) crystals developed within coarse-grained hornblende (am) phenocrystal; **c** acicular apatite (*ap*)

color, and frequently bent and/or granulated along the edges. The biotites of enclave and quartz diorite samples are rich in TiO_2 and MgO (Table 6), and plot within the calc-alkaline field defined by Nachit et al. (1985) (Fig. 11). $FeO_t/(FeO_t + MgO)$ ratio of biotite in MME is identical with biotite in host granite, suggesting that the biotites could be fully equilibrated with the host granite. In the host quartz diorite, the biotites have higher TiO_2 contents of average value of 4.97 wt%, whereas in the enclave biotite, TiO_2 decreases to average value of 3.54 wt%. This fact is probably due to simultaneous crystallization of abundant titanite in the MME, lowering the Ti activity during the hybridization.

Whole-rock geochemistry

A total of 80 rock samples were collected from the Karamadazı Granitoid, 32 of which, including granites, quartz diorite and MME, were analyzed for major, trace, and rare earth elements (Figs. 12, 13, 14, 15, 16, 17, 18). A selection of 15 representative analyses is given in Table 7. Major and trace elements were analyzed using inductively coupled plasma emission spectrometer from pulps after 0.2 g rock powder were fused with 1.5 g $LiBO_2$, and then dissolved in 100 mm^3 5% HNO_3. Rare earth elements were analyzed using inductively coupled plasma mass spectrometry from pulps after 0.25 g rock powder was dissolved with four acid digestions at ACME Analytical Laboratories Ltd., Vancouver, Canada. Analytical uncertainties range from 0.1 to 0.04% for major elements; from 0.1 to 0.5% for trace elements; and from 0.01 to 0.5 ppm for rare earth elements.

On the nomenclature diagram of Debon and Le Fort (1982), the MME and their host rocks plot in quartz diorite to gabbro/diorite fields, whereas leucogranites are found within adamellite and granite fields (Fig. 12), which is consistent with QAP in Fig. 3. The term ''adamellite'' is obsolete and monzogranite is used instead (Le Maitre et al. 1989). Ca-poor composition of the plagioclase of the MME and particularly their hosts are mostly less than 50% An, indicating dioritic composition. Most MME and quartz diorites plot in the calc-alkaline field in a K_2O versus SiO_2 diagram (Fig. 13). The granites display a slightly more potassic character by plotting within the medium-K field.

Total FeO_t has been chosen as the abscissa for the variation diagrams, because it more effectively discriminates between these granitic and mafic rocks than SiO_2 does (Figs. 14, 15). MME, quartz diorites and the granite display distinct ranges of SiO_2 contents (respectively 54–60, 60–63, and 75–78 wt%) (Figs. 13, 14; Table 7). No substantial overlap exists between the MME and the quartz diorites. A sample from quartz diorites seems to have anomalous values owing to analytical error or missampling. A distinct compositional gap in SiO_2 content (63–75 wt%) occurs between the quartz diorites and the granites. Most major elements (with the exception of K_2O, Na_2O, SiO_2) display positive correlation trends with FeO_t and smaller oxide variability with increasing FeO_t content

Table 2 Microprobe plagioclase analyses from quartz diorites

Sample no.	34				34				44				45				47				47			
	c	c/r	r	vr	c	c/r	r	vr	c	c/r	r	vr	c	c/r	r	vr	c	c/r	r	vr	c	c/r	r	vr
SiO_2	58.94	59.07	59.09	61.32	58.20	58.23	63.43	63.17	60.54	60.16	59.80	60.95	59.37	59.51	59.68	62.66	60.24	57.26	60.85	62.36	59.69	56.22	55.44	62.43
Al_2O_3	25.62	25.57	25.43	24.19	26.48	26.33	23.05	22.90	25.02	25.10	25.26	24.37	25.07	25.05	25.02	23.08	24.67	26.76	24.18	23.60	25.26	27.57	28.14	23.41
CaO	7.61	7.48	7.61	5.94	8.68	8.32	4.54	4.35	6.87	7.19	7.37	6.11	7.28	7.29	7.21	4.76	6.67	9.19	6.33	5.09	7.20	9.94	10.39	4.78
Na_2O	7.07	7.23	7.03	8.06	6.54	6.58	8.79	8.91	7.70	7.55	7.29	7.90	7.23	7.15	7.44	8.72	7.81	6.39	7.88	8.59	7.27	5.79	5.45	8.54
K_2O	0.21	0.32	0.27	0.22	0.15	0.36	0.33	0.23	0.17	0.18	0.25	0.18	0.28	0.32	0.23	0.26	0.10	0.13	0.34	0.15	0.32	0.21	0.18	0.36
Total	99.44	99.67	99.43	99.72	100.04	99.81	100.13	99.55	100.30	100.18	99.97	99.51	99.23	99.33	99.57	99.47	99.48	99.72	99.58	99.80	99.74	99.72	99.61	99.52
Si	7.928	7.929	7.944	8.179	7.795	7.816	8.393	8.402	8.048	8.018	7.992	8.150	7.990	7.999	8.009	8.356	8.078	7.716	8.146	8.296	7.990	7.593	7.501	8.320
Al	4.062	4.046	4.031	3.804	4.181	4.166	3.596	3.590	3.922	3.945	3.980	3.842	3.977	3.970	3.959	3.629	3.900	4.251	3.816	3.702	3.986	4.390	4.489	3.677
Ca	1.097	1.076	1.096	0.849	1.246	1.196	0.643	0.620	0.978	1.027	1.056	0.875	1.049	1.050	1.037	0.680	0.958	1.326	0.908	0.725	1.033	1.438	1.507	0.682
Na	1.844	1.882	1.832	2.085	1.699	1.712	2.255	2.298	1.985	1.951	1.889	2.048	1.887	1.863	1.936	2.255	2.031	1.669	2.046	2.216	1.888	1.516	1.431	2.208
K	0.036	0.055	0.046	0.037	0.025	0.061	0.055	0.039	0.029	0.030	0.043	0.030	0.048	0.055	0.039	0.044	0.017	0.021	0.059	0.026	0.054	0.036	0.031	0.062
Ab	62.0	62.5	61.6	70.2	57.2	57.7	76.4	77.7	66.3	64.9	63.2	69.3	63.2	62.8	64.3	75.7	67.6	55.3	67.9	74.7	63.5	50.7	48.2	74.8
An	36.8	35.7	36.8	28.6	42.0	40.3	21.8	21.0	32.7	34.1	35.3	29.6	35.2	35.4	34.4	22.8	31.9	44.0	30.2	24.4	34.7	48.1	50.7	23.1
Or	1.2	1.8	1.6	1.2	0.8	2.1	1.9	1.3	1.0	1.0	1.4	1.0	1.6	1.9	1.3	1.5	0.6	0.7	1.9	0.9	1.8	1.2	1.1	2.1
Sample no.	40				38				38				49				36				40			
	c	c/r	r	vr	c	c/r	r	vr	c	c/r	r	vr	c	c/r	r	vr	c	c/r	r	vr	c	c/r	r	vr
SiO_2	54.17	58.95	62.55	61.46	60.37	58.59	60.54	62.08	59.98	59.11	59.12	60.39	55.32	57.32	59.54	62.94	56.90	59.83	61.64	63.49	52.57	57.72	52.67	62.15
Al_2O_3	28.78	25.82	23.66	23.89	24.66	25.85	24.41	23.83	24.89	25.71	25.45	24.68	28.17	26.76	25.38	23.08	27.00	25.18	23.76	23.00	30.27	26.92	30.35	23.81
CaO	11.57	7.77	5.01	5.43	6.68	8.06	6.45	5.44	6.93	7.71	7.60	6.62	10.81	9.16	7.59	4.67	9.51	7.30	5.64	4.57	13.45	8.97	13.34	5.32
Na_2O	4.91	6.99	8.61	8.36	7.56	6.68	7.66	8.54	7.44	7.03	7.13	7.57	5.45	6.32	7.09	8.86	6.15	7.28	8.16	8.83	3.95	6.33	3.94	8.52
K_2O	0.09	0.17	0.16	0.12	0.30	0.25	0.28	0.13	0.21	0.20	0.27	0.27	0.11	0.21	0.19	0.16	0.19	0.30	0.32	0.21	0.10	0.19	0.12	0.21
Total	99.52	99.69	99.99	99.26	99.56	99.43	99.34	100.01	99.46	99.76	99.58	99.52	99.86	99.76	99.79	99.70	99.75	99.89	99.53	100.10	100.33	100.14	100.42	100.01
Si	7.359	7.910	8.300	8.227	8.086	7.882	8.118	8.250	8.041	7.923	7.940	8.088	7.476	7.719	7.972	8.371	7.674	8.000	8.233	8.401	7.121	7.736	7.120	8.257
Al	4.611	4.084	3.700	3.769	3.894	4.099	3.859	3.734	3.934	4.063	4.029	3.896	4.487	4.248	4.007	3.618	4.294	3.970	3.742	3.588	4.835	4.254	4.838	3.730
Ca	1.685	1.117	0.712	0.779	0.958	1.162	0.927	0.775	0.996	1.107	1.094	0.950	1.565	1.321	1.088	0.666	1.374	1.046	0.808	0.647	1.952	1.289	1.933	0.757
Na	1.292	1.818	2.214	2.170	1.964	1.742	1.992	2.200	1.935	1.826	1.857	1.964	1.428	1.649	1.841	2.285	1.609	1.887	2.114	2.265	1.036	1.644	1.033	2.195
K	0.015	0.029	0.027	0.020	0.051	0.042	0.048	0.021	0.037	0.034	0.047	0.045	0.019	0.037	0.033	0.026	0.033	0.052	0.054	0.036	0.017	0.033	0.020	0.035
Ab	43.2	61.3	75.0	73.1	66.0	59.1	67.2	73.4	65.2	61.6	62.0	66.4	47.4	54.8	62.2	76.8	53.4	63.2	71.0	76.8	34.5	55.4	34.6	73.5
An	56.3	37.7	24.1	26.2	32.2	39.4	31.2	25.9	33.6	37.3	36.5	32.1	52.0	43.9	36.7	22.4	45.6	35.0	27.1	22.0	64.9	43.5	64.7	25.4
Or	0.5	1.0	0.9	0.7	1.7	1.4	1.6	0.7	1.2	1.1	1.6	1.5	0.6	1.2	1.1	0.9	1.1	1.7	1.8	1.2	0.6	1.1	0.7	1.2

Abbreviations: *c* core; *c/r* core to rim; *r* rim; *vr* very rim

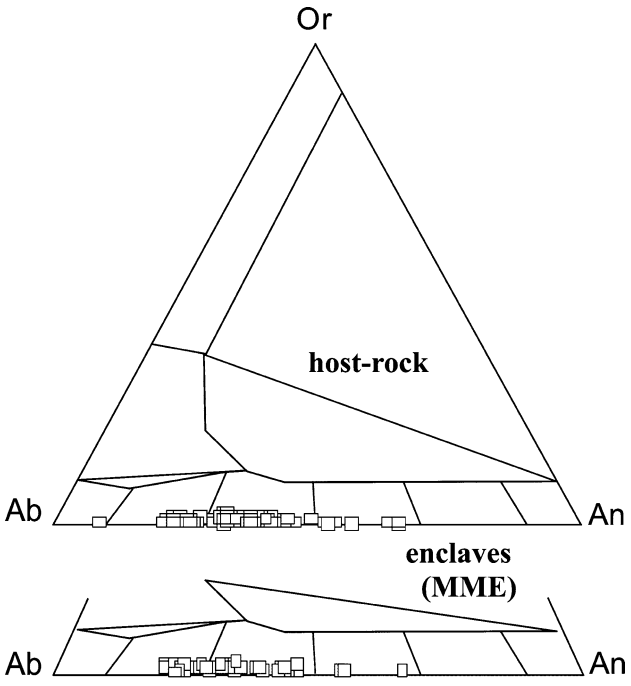

Fig. 6 Chemical compositions of plagioclase from the host rock and enclave

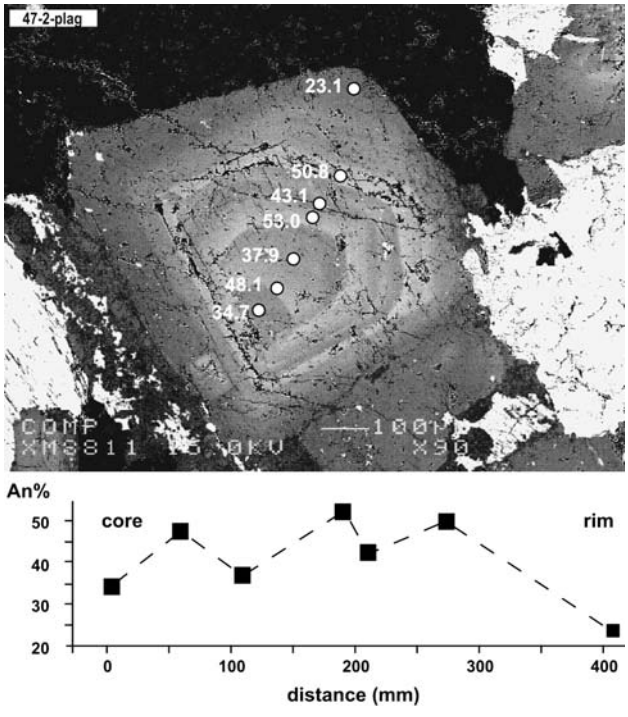

Fig. 7 Back-scatter view of electron image oscillatory zoning in plagioclase from quartz diorite (*top*). Zoning pattern (An% composition) from core to rim in the same plagioclase (*bottom*)

though. K_2O has positive and negative correlation trends for quartz diorites, and enclaves, respectively. Na_2O+K_2O show linear trends in quartz diorites and

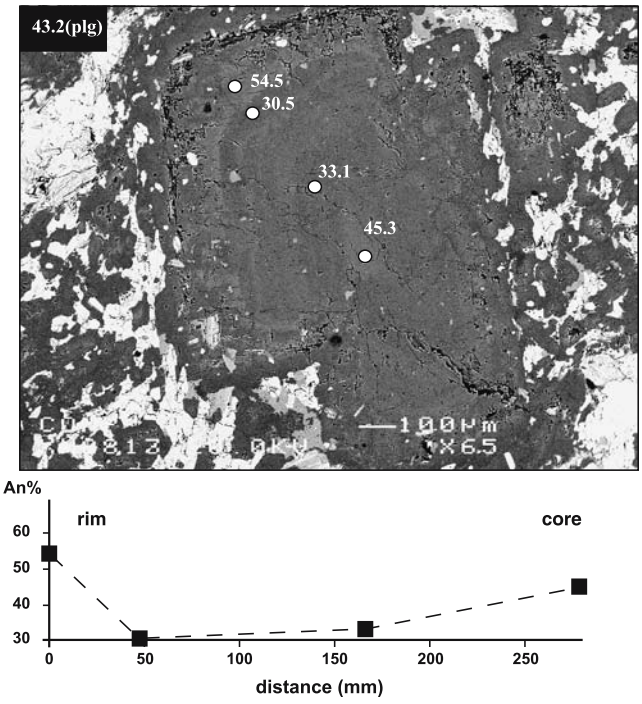

Fig. 8 Back-scatter view of reverse zoning in plagioclase from enclave, and zoning pattern (An% composition) in the same plagioclase

enclaves, suggesting variation is in compositional proportions of feldspars. The trend of Al_2O_3 versus FeO_t appears positive for leucogranites and not clear for quartz diorite and MME. Other oxide trends are mostly linear. The quartz diorites and granites have mean ASI [aluminum saturation index, molecular $Al_2O_3/(CaO+Na_2O+K_2O)$] values of 0.84 and 1.05, respectively, and are therefore metaluminous and slightly peraluminous. MME have similar ASI values, 0.80, to their hosts.

Trace elements display trends with FeO_t content less well defined than major elements (Fig. 15). Cr, Ni, Co, Sc, Cu, Sr, and Y tend to be present at higher concentrations in the MME and quartz diorites than in granites (Fig. 15 and Table 7). Rb, U and Th are more abundant in the granites than in the MME and quartz diorites. Sr follows Na_2O and Rb follows K_2O.

The chondrite-normalized rare earth element (REE) diagrams show that MME and quartz diorites have broadly similar, slightly concave-upward patterns (Fig. 16). Some MME have a slight negative Eu anomaly, indicating plagioclase fractionation. In comparison with quartz diorite, they have slightly higher $(La/Lu)_N$ ratios, indicating REE fractionation, and lower LREE content. The granite REE patterns are mostly characterized by negative Eu ($Eu/Eu^* = 0.39$–0.96) anomalies, positive REE fractionation from Eu

Table 3 Microprobe plagioclase analyses from enclaves

Sample no.	47				40				49-1				43				49-1				43			
	c	c/r	r	vr	c	c/r	r	vr	c	c/r	r	vr	c	c/r	r	vr	c	c/r	r	vr	c	c/r	r	vr
SiO_2	55.00	60.19	60.19	62.86	57.49	60.23	59.99	61.30	58.41	60.23	62.42	63.43	60.75	58.45	62.66	62.44	56.84	57.71	59.75	61.49	56.88	60.16	60.59	54.75
Al_2O_3	28.62	25.45	25.04	23.15	26.60	24.80	24.93	24.26	26.01	24.86	23.46	22.76	24.73	25.91	23.20	23.30	27.32	26.79	25.29	24.15	26.95	24.72	24.41	28.50
CaO	11.22	7.10	6.87	4.65	9.19	6.73	7.03	5.97	8.00	6.84	4.97	4.24	6.61	7.89	4.87	4.80	9.67	9.06	7.23	5.89	9.34	6.89	6.42	11.38
Na_2O	5.25	7.64	7.46	8.84	6.27	7.67	7.41	8.11	6.87	7.61	8.60	9.13	7.78	6.88	8.67	8.85	6.17	6.46	7.31	8.20	6.04	7.38	7.88	5.16
K_2O	0.14	0.15	0.29	0.30	0.15	0.21	0.23	0.17	0.16	0.22	0.32	0.18	0.18	0.22	0.14	0.10	0.15	0.18	0.22	0.20	0.30	0.47	0.29	0.14
Total	100.23	100.52	99.85	99.79	99.71	99.64	99.59	99.81	99.45	99.76	99.76	99.73	100.05	99.33	99.54	99.49	100.15	100.19	99.80	99.92	99.51	99.61	99.59	99.92
Si	7.416	7.994	8.044	8.353	7.741	8.064	8.040	8.169	7.861	8.054	8.304	8.425	8.094	7.873	8.349	8.324	7.636	7.738	7.996	8.187	7.682	8.061	8.111	7.407
Al	4.549	3.984	3.945	3.627	4.223	3.915	3.939	3.812	4.126	3.920	3.680	3.564	3.885	4.114	3.644	3.662	4.327	4.235	3.989	3.790	4.291	3.905	3.852	4.546
Ca	1.621	1.010	0.984	0.662	1.326	0.966	1.009	0.852	1.154	0.980	0.708	0.603	0.944	1.139	0.696	0.685	1.393	1.301	1.037	0.840	1.352	0.989	0.920	1.649
Na	1.373	1.967	1.933	2.277	1.638	1.990	1.924	2.095	1.793	1.973	2.219	2.351	2.011	1.796	2.239	2.288	1.607	1.678	1.897	2.117	1.583	1.918	2.046	1.352
K	0.025	0.025	0.049	0.051	0.026	0.036	0.039	0.028	0.028	0.038	0.054	0.030	0.030	0.037	0.024	0.016	0.026	0.031	0.038	0.034	0.051	0.081	0.049	0.024
Ab	45.5	65.5	65.2	76.2	54.8	66.5	64.7	70.4	60.3	66.0	74.4	78.8	67.4	60.4	75.7	76.5	53.1	55.8	63.8	70.8	53.0	64.2	67.8	44.7
An	53.7	33.7	33.2	22.1	44.3	32.3	33.9	28.6	38.8	32.8	23.8	20.2	31.6	38.3	23.5	22.9	46.0	43.2	34.9	28.1	45.3	33.1	30.5	54.5
Or	0.8	0.8	1.7	1.7	0.9	1.2	1.3	0.9	0.9	1.3	1.8	1.0	1.0	1.2	0.8	0.5	0.8	1.0	1.3	1.1	1.7	2.7	1.6	0.8

Abbreviations: c core; *c/r* core to rim; *r* rim; *vr* very rim

to La (LREE), and a negative fractionation from Lu to Eu (HREE).

The primitive mantle-normalized diagrams (spidergrams) show consistent patterns within each rock type. The spidergrams display prominent negative Ba, Nb, and TiO_2 anomalies in the granites (Fig. 17). The Pb anomaly is positive in the granite but negative in the quartz diorite and MME. All samples have a characteristic negative Nb anomaly, which suggests a subduction component in their genesis (Pearce 1983).

Discussion and petrogenetic approach

The source of MME in granitic plutons has been and is still a fundamental petrologic question. Various sources, ranging from early cumulates (e.g., Dodge and Kistler 1990) to disrupted mafic dikes (e.g., Pitcher 1991), have been established in different plutons. A major implication of the existence of MME is the potential chemical modification of its granitic host. Hence, the petrogenesis of a granitic suite cannot be fully understood without assessing the origin of its MME.

Quartz diorites (SiO_2 = 60–63 wt%; Al_2O_3 = 17–20 wt%) have many characteristics of adakites; high Na_2O (4.1≥ wt%), Na_2O/K_2O (≥1.6), Sr (>600 ppm), LREE (La, mostly >24 ppm), low Y (≤17 ppm) and HREE (Yb≤1.85 ppm), and high Sr/Y (>40) with positive Sr anomalies in Fig. 17c. However, they show lower Mg# [(molar 100 × MgO/(MgO + FeO_t)) < 0.59], Ni (~7 ppm), and Cr (~45 ppm) contents (Fig. 18) than that of adakites, which could be interpreted as reflecting lack of, or a lower degree of, interaction between their parental magma and the overlying mantle wedge. Quartz diorites also differ from adakites in terms of fluid-mobile trace elements, such as K (1.6 wt%), Ba (~417 ppm), and Rb (~46 ppm). The relatively high contents of these elements in quartz diorites compared with adakites may reflect a subduction zone component in quartz diorite sources, which is not present in the descending slab source of adakites (Defant and Drummond 1990, 1993). TTGs (tonalite–trondhjemite–granodiorite) show chemical characteristics of adakites, but they are lesss mafic and can be distinguished from adakites by their relatively low Ni, Cr (Fig. 18), Mg#, and high Ba, K, Rb. Hence, geochemical characteristics of the quartz diorites studied here resemble mostly to high-Al TTGs, which could be formed by partial melting of a wet mafic protolith of the lower crust in arc systems (Rapp et al. 1991; Smithies 2000; Prouteau et al. 2001; Condie 2005).

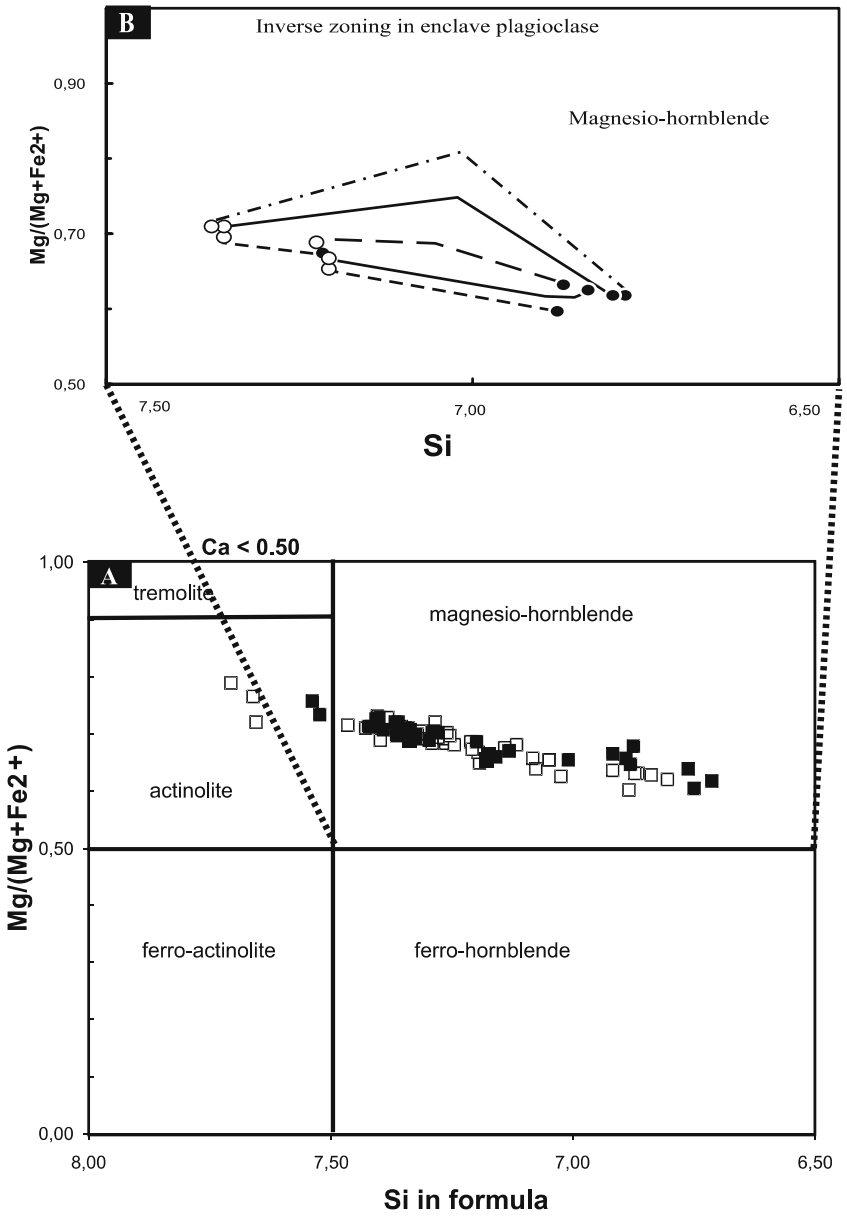

Fig. 9 **a** Composition and classification (Leake et al. 1997) of amphiboles from the host rock and enclave; **b** inverse zoning in enclave hornblendes. *Filled* and *open circles* represent core and rim of the crystals, respectively

Magmatic textures, mineralogy, and chemical features of MME show that they crystallized from a relatively mafic magma of intermediate composition. Since MME are metaluminous in composition, and do not contain peraluminous minerals, they are possibly not restites and cannot have formed by transformation of the residues of partial melting of crustal rocks. Similarity of enclave–host mineralogy/chemistry, and lack of enclaves with large crystals and cumulate textures preclude an autolith origin for MME from early disruption of cumulate layers in the intrusion. Thus, MME are possibly globules of a more mafic magma, mingled with host magma. The cogenetic nature of MME and host granitoids are shown by (a) similar mineral assemblages and mineral compositions, (b) existence of strong correlations between major and trace elements in MME and hosts, although concentrations of major and trace elements are different. Field relationships, for example, the coeval nature of the enclaves and quartz diorites and the existence of widespread mafic enclaves (Fig. 2a), clearly propose magma mixing between mafic and felsic magmas. This is supported by the occasional presence of textural and compositional disequilibrium displayed by plagioclase xenocrysts in the MME. However, several major and trace elements, such as FeO_t, Na_2O, K_2O, Ba, and Sr (Figs. 14, 15), show non-linear variations, which are difficult to interpret in terms of simple linear mixing. Among these, FeO_t versus Ba and Sr (Fig. 15) is of particular interest, in which Ba and Sr contents vary

Table 4 Microprobe hornblende analyses from quartz diorites

Sample no.	34-1		34-3		38-2		44-4		36-16		45-8			34-2	38-27		43-41	
	c	r	c	r	c	r	c	r	c	r	c	c/r	r	c	c	r	c	r
SiO_2	50.79	50.75	51.44	51.40	50.70	50.64	50.80	50.54	50.98	50.84	46.99	46.70	49.99	44.41	48.11	48.12	47.75	50.21
TiO_2	0.81	0.83	0.64	0.76	0.79	0.76	0.76	0.77	0.73	0.74	1.34	1.38	0.91	0.00	0.00	0.00	1.40	0.62
Al_2O_3	4.72	4.60	4.03	4.03	4.94	4.72	4.26	4.39	4.29	4.49	7.45	8.14	4.80	9.34	6.49	6.54	6.67	5.24
Cr_2O_3	0.00	0.00	0.04	0.00	0.00	0.00	0.01	0.05	0.00	0.03	0.00	0.00	0.02	0.06	0.00	0.01	0.06	0.22
Fe_2O_3	0.94	1.34	1.04	0.90	0.76	1.18	2.07	2.11	0.95	1.42	1.37	0.01	0.57	3.13	5.87	5.88	0.87	1.20
FeO	10.80	10.59	10.34	10.91	11.39	11.30	9.51	9.96	10.84	9.99	11.67	12.02	11.90	11.70	8.13	7.83	12.61	10.60
MnO	0.36	0.31	0.34	0.35	0.36	0.39	0.37	0.35	0.32	0.27	0.30	0.31	0.34	0.36	0.37	0.36	0.38	0.36
MgO	16.05	16.01	16.76	16.33	15.82	15.59	16.35	16.16	15.95	16.28	14.29	14.26	15.33	12.38	14.47	14.65	14.28	15.61
CaO	12.18	12.37	12.11	12.12	11.96	12.20	12.41	12.29	12.36	12.39	12.16	12.12	12.13	12.11	12.02	12.02	11.99	12.34
Na_2O	0.74	0.73	0.81	0.71	0.72	0.72	0.64	0.70	0.70	0.67	1.27	1.40	0.89	1.37	0.00	0.00	1.16	0.76
K_2O	0.39	0.41	0.36	0.32	0.42	0.40	0.35	0.41	0.37	0.38	0.65	0.71	0.46	1.07	0.61	0.61	0.66	0.41
Total	97.77	97.94	97.91	97.83	97.84	97.89	97.52	97.71	97.49	97.50	97.47	97.03	97.34	95.91	96.07	96.03	97.83	97.57
Si	6.350	6.346	6.408	6.416	6.342	6.349	6.372	6.346	6.394	6.367	5.986	5.947	6.313	5.840	6.212	6.208	6.063	6.305
Ti	0.077	0.078	0.060	0.072	0.074	0.072	0.072	0.073	0.069	0.070	0.128	0.132	0.086	0.000	0.000	0.000	0.134	0.058
Al	0.695	0.679	0.591	0.594	0.728	0.698	0.629	0.650	0.635	0.663	1.119	1.222	0.715	1.448	0.988	0.995	0.999	0.776
Cr	0.000	0.000	0.004	0.000	0.000	0.000	0.001	0.005	0.000	0.003	0.000	0.000	0.002	0.006	0.000	0.001	0.006	0.022
Fe^{3+}	0.088	0.126	0.097	0.084	0.072	0.111	0.195	0.199	0.090	0.133	0.132	0.001	0.055	0.310	0.570	0.571	0.083	0.114
Fe^{2+}	1.129	1.107	1.077	1.138	1.191	1.185	0.998	1.046	1.137	1.046	1.243	1.280	1.257	1.287	0.878	0.845	1.339	1.114
Mn	0.038	0.033	0.036	0.037	0.038	0.042	0.039	0.037	0.034	0.029	0.032	0.033	0.036	0.040	0.040	0.039	0.041	0.038
Mg	2.991	2.984	3.112	3.038	2.948	2.912	3.057	3.023	2.981	3.038	2.713	2.706	2.885	2.426	2.785	2.817	2.702	2.920
Ca	1.631	1.657	1.617	1.621	1.603	1.638	1.668	1.653	1.661	1.663	1.659	1.654	1.641	1.707	1.664	1.661	1.632	1.660
Na	0.179	0.177	0.196	0.173	0.174	0.175	0.155	0.171	0.171	0.163	0.312	0.344	0.218	0.293	0.000	0.000	0.286	0.185
K	0.063	0.065	0.058	0.052	0.067	0.064	0.057	0.065	0.059	0.061	0.106	0.115	0.075	0.179	0.101	0.101	0.108	0.066
Mg#	0.726	0.729	0.743	0.727	0.712	0.711	0.754	0.743	0.724	0.744	0.686	0.679	0.697	0.653	0.760	0.769	0.669	0.724

Abbreviations: c core; *c/r* core to rim; *r* rim

Mg#: molar $100 \times (Mg/Mg + Fe^{2+})$

Table 5 Microprobe hornblende analyses from the enclaves

Sample no.	38-25		38-26		40-22		40-23		44-42			47-10		49-33		N36-15		47-11	
	c	r	c	r	c	r	c	r	c	c/r	r	c	r	c	r	c	r	c	r
SiO_2	50.63	50.53	45.13	48.41	46.42	48.94	45.75	50.67	50.88	50.51	49.16	51.15	48.12	53.59	54.30	51.25	49.98	50.30	48.47
TiO_2	0.78	0.86	0.00	0.00	1.79	0.92	1.58	0.84	0.78	0.81	0.84	0.83	1.29	0.31	0.23	0.74	0.49	0.83	1.25
Al_2O_3	4.68	4.77	8.73	5.90	8.31	5.70	8.14	4.56	4.50	4.49	5.55	4.49	6.58	2.52	1.97	4.23	5.23	4.74	6.11
Cr_2O_3	0.00	0.00	0.00	0.03	0.02	0.00	0.00	0.03	0.02	0.00	0.05	0.00	0.00	0.01	0.05	0.03	0.00	0.01	0.05
Fe_2O_3	1.46	1.19	7.30	2.91	0.33	1.45	0.57	0.85	1.62	1.80	1.70	0.70	1.24	0.07	0.58	0.78	1.53	1.14	1.49
FeO	10.74	11.26	8.47	11.13	13.48	11.61	13.89	10.93	10.18	10.15	11.30	10.34	12.29	9.65	8.32	10.15	11.10	11.26	12.27
MnO	0.35	0.38	0.31	0.35	0.31	0.39	0.40	0.37	0.37	0.38	0.38	0.36	0.37	0.23	0.26	0.34	0.35	0.36	0.35
MgO	16.14	15.58	12.68	14.34	13.11	14.57	13.19	16.00	16.21	16.06	14.89	16.48	14.32	17.71	18.61	16.43	15.18	15.88	14.60
CaO	12.11	12.33	11.87	12.13	12.11	12.24	11.55	12.12	12.23	12.15	12.17	12.08	12.09	12.55	12.73	12.42	12.39	12.16	12.00
Na_2O	0.86	0.78	0.00	0.96	1.10	0.78	1.47	0.74	0.64	0.65	0.80	0.64	1.01	0.52	0.50	0.66	0.80	0.81	1.04
K_2O	0.41	0.40	0.90	0.60	0.78	0.55	0.78	0.43	0.38	0.38	0.53	0.36	0.64	0.22	0.17	0.39	0.47	0.43	0.61
Total	98.16	98.08	95.39	96.76	97.75	97.15	97.30	97.53	97.81	97.36	97.36	97.42	97.94	97.36	97.71	97.42	97.52	97.90	98.23
Si	6.327	6.328	5.956	6.223	5.916	6.225	5.888	6.356	6.363	6.354	6.236	6.387	6.097	6.626	6.666	6.406	6.307	6.097	6.127
Ti	0.073	0.081	0.000	0.000	0.171	0.088	0.152	0.080	0.073	0.076	0.080	0.078	0.123	0.029	0.021	0.070	0.046	0.123	0.119
Al	0.690	0.705	1.359	0.894	1.248	0.855	1.234	0.674	0.663	0.665	0.830	0.660	0.983	0.367	0.285	0.623	0.779	0.983	0.911
Cr	0.000	0.000	0.000	0.003	0.002	0.000	0.000	0.003	0.002	0.000	0.005	0.000	0.000	0.001	0.005	0.003	0.000	0.000	0.005
Fe^{3+}	0.138	0.112	0.685	0.282	0.032	0.139	0.055	0.080	0.153	0.171	0.162	0.066	0.119	0.006	0.053	0.073	0.146	0.119	0.142
Fe^{2+}	1.123	1.180	0.935	1.196	1.437	1.236	1.495	1.147	1.064	1.068	1.199	1.080	1.302	0.998	0.854	1.061	1.172	1.302	1.297
Mn	0.037	0.040	0.034	0.038	0.034	0.041	0.043	0.039	0.039	0.041	0.041	0.038	0.040	0.024	0.027	0.036	0.037	0.040	0.038
Mg	3.005	2.907	2.495	2.748	2.490	2.762	2.530	2.990	3.021	3.011	2.815	3.068	2.703	3.264	3.405	3.061	2.854	2.703	2.752
Ca	1.622	1.654	1.679	1.671	1.654	1.669	1.593	1.629	1.639	1.638	1.654	1.616	1.642	1.662	1.674	1.663	1.675	1.642	1.625
Na	0.207	0.189	0.000	0.240	0.271	0.192	0.367	0.179	0.155	0.157	0.196	0.154	0.247	0.124	0.119	0.160	0.197	0.247	0.254
K	0.065	0.064	0.152	0.098	0.127	0.090	0.127	0.068	0.060	0.061	0.086	0.058	0.103	0.034	0.027	0.062	0.075	0.103	0.098
Mg#	0.728	0.711	0.727	0.697	0.634	0.691	0.629	0.723	0.740	0.738	0.701	0.740	0.675	0.766	0.799	0.743	0.709	0.675	0.680

Abbreviations: c core; *c/r* core to rim; *r* rim

Mg#: molar $100 \times (Mg/Mg + Fe^{2+})$

Table 6 Microprobe pyroxene and biotite analyses from the host rock and enclave

Pyroxene							Biotite					
	Enclave							Host rock		Enclave		
Sample no.	49						Sample no.	34-1		45-2	40-4	44-3
	c	r	c	r	c	r		c	r	c	c	c
SiO_2	54.10	53.92	53.52	53.48	52.82	54.01	SiO_2	37.38	37.20	36.30	37.35	34.81
TiO_2	0.10	0.11	0.20	0.10	0.13	0.13	TiO_2	5.08	4.855	2.915	3.625	4.073
Al_2O_3	0.00	0.00	1.05	0.00	0.00	1.22	Al_2O_3	13.85	13.82	14.34	14.31	13.32
Cr_2O_3	0.00	0.00	0.04	0.00	0.02	0.00	Cr_2O_3	0.00	0.02	0.01	0.00	0.05
Fe_2O_3	1.23	1.28	1.77	1.79	2.32	1.18	FeOt	15.91	16.24	17.57	17.81	17.39
FeO	4.12	5.87	4.11	6.10	5.69	3.53	MnO	0.17	0.18	0.25	0.17	0.24
MnO	0.20	0.25	0.23	0.34	0.33	0.18	MgO	14.02	13.81	14.40	12.84	13.15
MgO	15.27	14.29	14.83	14.22	13.93	15.32	CaO	0.02	0.00	0.09	0.07	0.00
CaO	24.71	24.09	24.47	23.71	23.85	24.95	Na_2O	0.13	0.12	0.03	0.07	0.07
Na_2O	0.39	0.50	0.58	0.50	0.57	0.44	K_2O	10.16	9.92	8.49	10.14	8.34
K_2O	0.02	0.01	0.00	0.00	0.00	0.00	Total	96.76	96.19	94.44	96.42	91.47
Total	100.14	100.31	100.79	100.23	99.66	100.96	Si	5.560	5.569	5.534	5.618	5.505
Si	1.990	1.994	1.958	1.984	1.972	1.965	Ti	0.569	0.547	0.334	0.410	0.484
Ti	0.003	0.003	0.005	0.003	0.004	0.003	Al	2.430	2.440	2.577	2.538	2.483
Al	0.000	0.000	0.045	0.000	0.000	0.052	Cr	0.000	0.003	0.002	0.000	0.007
Cr	0.000	0.000	0.001	0.000	0.001	0.000	Fe^{2+}	1.980	2.034	2.241	2.240	2.300
Fe^{3+}	0.043	0.043	0.068	0.063	0.089	0.042	Mn	0.022	0.023	0.033	0.022	0.033
Fe^{2+}	0.118	0.175	0.107	0.176	0.154	0.098	Mg	3.108	3.083	3.273	2.878	3.100
Mn	0.006	0.008	0.007	0.011	0.010	0.006	Ca	0.004	0.000	0.016	0.012	0.000
Mg	0.837	0.787	0.809	0.786	0.775	0.830	Na	0.039	0.035	0.011	0.021	0.023
Ca	0.974	0.954	0.959	0.942	0.954	0.973	K	1.929	1.896	1.652	1.947	1.684
Na	0.028	0.036	0.041	0.036	0.041	0.031						
K	0.001	0.000	0.000	0.000	0.000	0.000						

Abbreviations : c core; *r* rim

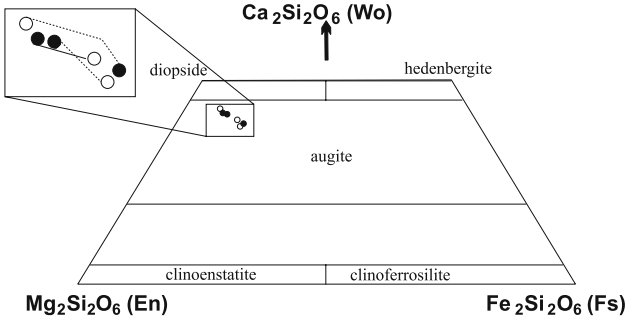

Fig. 10 Wo–En–Fs composition plot of pyroxene from enclave (after Morimoto 1988). *Filled* and *open circles* represent core and rim of the crystals, respectively

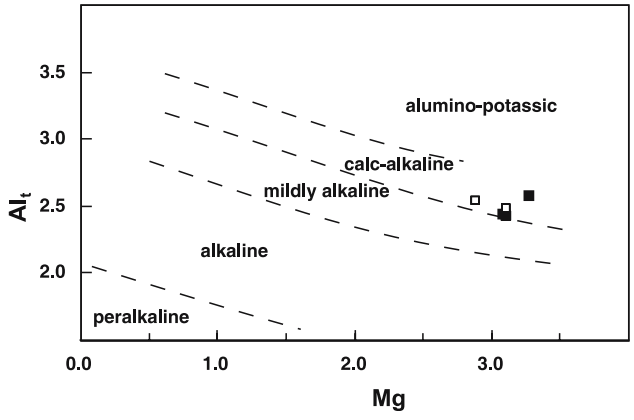

Fig. 11 Mg versus Al_t atoms (*pfu*) plot of biotite from the host rock (*filled square*) and enclave (*open square*). Dividing lines and fields are from Nachit et al. (1985)

substantially for little change in FeO_t in quartz diorites. Dispersion on the diagrams is of paramount evidence of K-feldspar 'cumulus'. Small amount of K-feldspars may induce an increase in Ba and Sr contents in quartz diorites owing to their high partition coefficients (K_D) for Ba, [5.37, López-Ruiz and Cebria (1990); 5.9, López-Moro (2000)], and for Sr (3.87; López-Ruiz and Cebria 1990). Plagioclase has low K_D for Ba (0.36, López-Ruiz and Cebria 1990), therefore is unlikely to cause this enrichment. Accordingly, some samples from quartz diorite are low in SiO_2 (>57 wt%) and ASI (<0.85), indicating a cumulate origin for these samples (Chappell and White 1992). Slightly high Eu/Eu* (1.02–1.11) and modally high plagioclase (up to 61%) contents in these samples may reflect existence of cumulus plagioclases. Existince of biotite cumulus in both quartz diorite and MME is suggested by dispersion of Rb (Fig. 15). In comparing with their hosts,

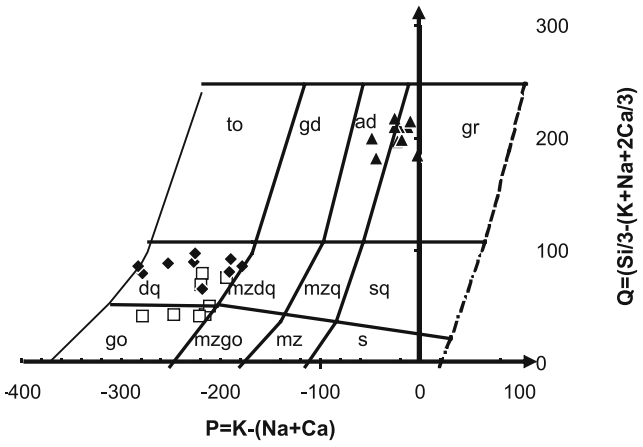

Fig. 12 Distribution of the samples in the nomenclature diagram for igneous rocks (Debon and Le Fort 1982). Parameters are expressed as gram-atom × 10,000. *Filled triangles*, *open squares* and *filled diamonds* represent granites, enclaves, and quartz diorites, respectively. *Abbreviations: gr* granite, *ad* adamellite, *gd* granodiorite, *to* tonalite, *sq* quartz syenite, *mzq* quartz-monzonite, *mzdq* quartz monzodiorite, *dq* quartz diorite (quartz gabbro-quartz anortozite), *s* syenite, *mz* monzonite, *mzgo* monzogabbro (monzodiorite), *go* gabbro (diorite-anortozite)

MME are usually enriched in P, Ti, Y, Nb, and HREE. This could be explained by selective interdiffusion of these elements into the less polymerized magmas. These elements were subsequently concentrated in apatite, titanite, and hornblendes due to their high K_D for these elements (López-Ruiz and Cebria 1990; Klein et al. 1997), maintaining their low activity in the melt. Such low activity in the mafic melt leads to the continuity of 'Uphill' diffusion, as described for K due to crystallization of biotite by Johnston and Wyllie (1988). Selective diffusion of these elements may be attributed to subsolidus reequilibration, which was supported by crystallization of anhedral titanite in MME in relation with hornblende, and existence of compositional zoning in quartz diorite (Fig. 2b), related to margins of MME. The diffusion may also be an earlier process under liquidus temperatures as suggested by the igneous habit of apatite (Fig. 5c).

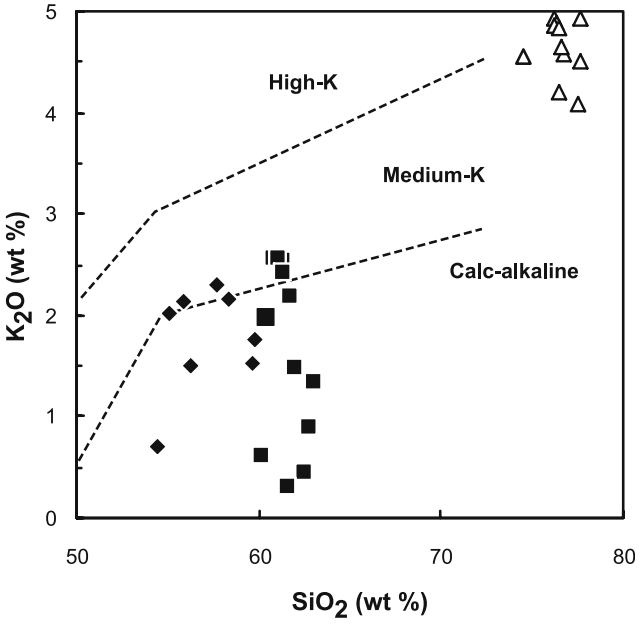

Fig. 13 A plot of SiO_2 versus K_2O showing calc-alkaline character of the granitoids. Dividing lines in K_2O versus SiO_2 plot is after Peccerillo and Taylor (1976). *Open triangles*, *filled diamonds* and *filled squares* represent granites, enclaves, and quartz diorites, respectively

Some evidence of local magma mingling is shown by the enclave structures. In particular, plagioclase and quartz crystals lay across the enclave contacts in some points, and rare, enclave–host gradational contacts locally occur (Fig. 2c), indicating that enclaves and their hosts simultaneously behaved as magmas at some stage in their histories. Mechanical accretion of early-crystallized phases from granitic host liquid into the mafic magma batch, carried trace elements with high K_D and their major components (e.g., Ca, Na, Sr, and Si, for feldspar and quartz).

MME and quartz diorites have low Nb/U (~6.01, ~5.66) ratios, similar to those of continental crust (Nb/U: 6.2; Rudnick and Fountain 1995), but distinct from those of mid-ocean ridge and oceanic island arc basalts (Nb/U: 47, Hofmann et al. 1986). Besides, they have negative Nb anomalies, and are enriched in large ion lithophile elements (LILEs) and light REEs (Fig. 16). All these features propose that the parental magmas have been contaminated by continental crust during magma ascent.

Samples from leucogranites are strongly enriched in SiO_2, Al_2O_3, K_2O ($Na_2O/K_2O < 1$), Rb, Th, U, Rb/Sr, La, and depleted in MgO, MnO, TiO_2, Ba, Sr, Nb. They are characterized by concave upward shape of the REE patterns, which is consistent with (1) the amphibole-out boundary not being crossed during partial melting (Romick et al. 1992) leaving amphibole as a major restite phase and (2) garnet not a major fractionating phase. High-SiO_2 granites also have low values of Eu/Eu* and Sr/Nd and low abundance of Sr, which requires significant amount of plagioclase in their residues during magma segregation, or plagioclase fractionation. I-type mineralogical and chemical features of Karamadazı granitoids (Chappell and White 1974), such as, for example, lack of muscovite, high Na_2O/K_2O ratio and low A/CNK (< 1.1) suggest that they could be derived from quartz diorites or even less evolved magmas by crystal fractionation. Aplitic

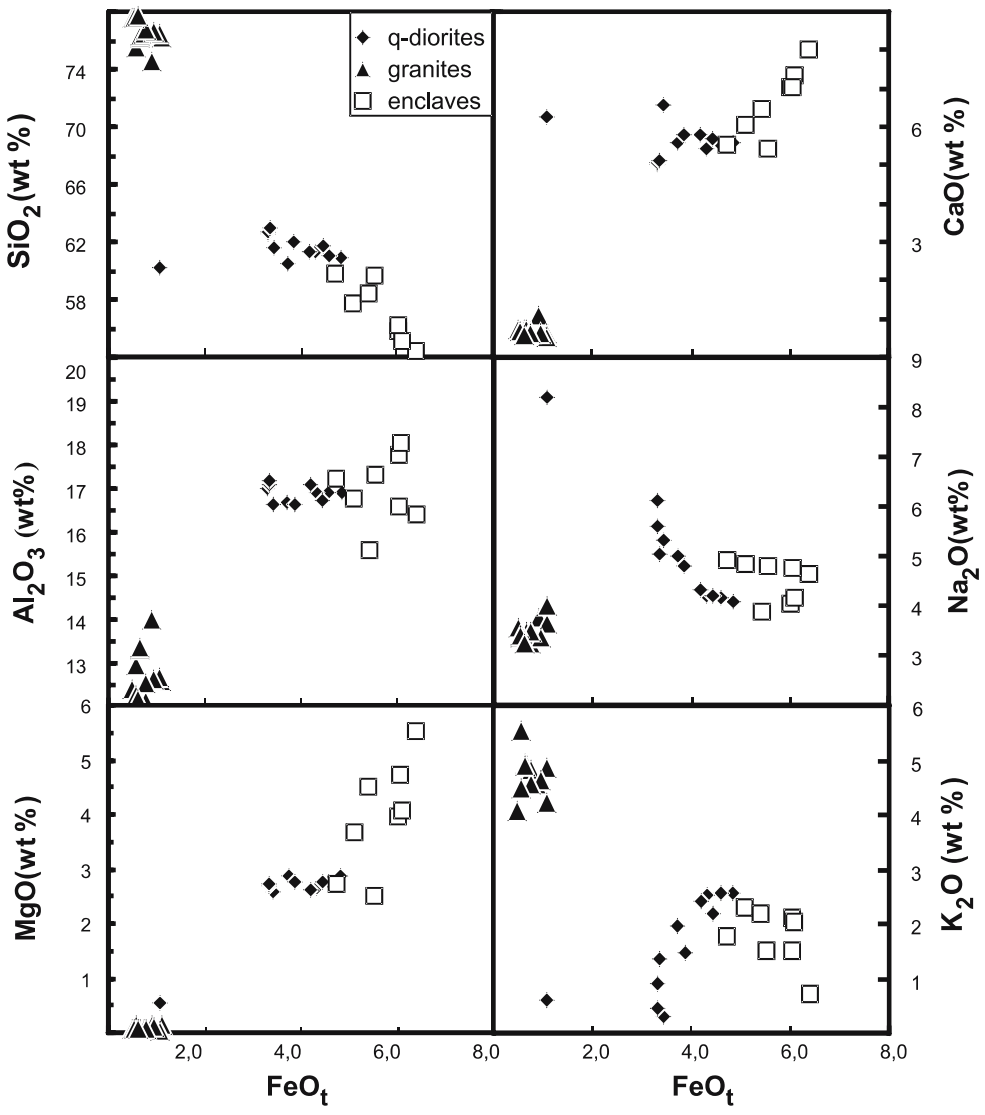

Fig. 14 FeO_t versus some major oxide element variation plots for host rock (*filled diamond*), enclave (*open square*), and granite (*filled triangle*) samples

dike suites on Karamadazı Granitoid most probably represent such co-magmatic highly differentiated late-stage melts. However, large volumes of granites relative to quartz diorite, and absence of samples with intermediate compositions in the field are not in favor of this suggestion. A multi-stage process may be required for the production of felsic granites, beginning with initial emplacement and/or underplating of mantle-derived melts into the crust. However, it is uncertain whether such rocks alone are adequately enriched in quartz and K and other LILE to be capable of creating true granitic melts; most experimental evidence suggests that partial melting of basaltic and other low-K rocks will produce mainly sodic melts, such as tonalites, trondhjemites, and sodic granodiorites (e.g., Rutter and Wyllie 1988; Rushmer 1990; Rapp et al. 1991). Crystal fractionation and contamination processes, which may have operated individually or together, seem to be required to make these mantle-derived melts more fertile. The granites display a small chemical variation, suggesting that they crystallized from a homogeneous magma and that fractional crystallization was minor during magma ascent. Therefore, leucogranites could be formed by partial melting of a predominantly intermediate protolith, coupled contamination, and minor feldspar-dominated fractionation.

MME, quartz diorites, and leucogranites are generally enriched in LILEs, and depleted in high-field strength elements (HFSE) (Fig. 17a, b), which are typical of arc magmatism (e.g., Parada et al. 1999; Shaw et al. 1993). An active continental margin setting conforms to the calc-alkaline character of the quartz diorite, with lower crust in origin. I favor a scenario in which intrusion of mantle-derived mafic magmas into thickened continental crust induced dehydration

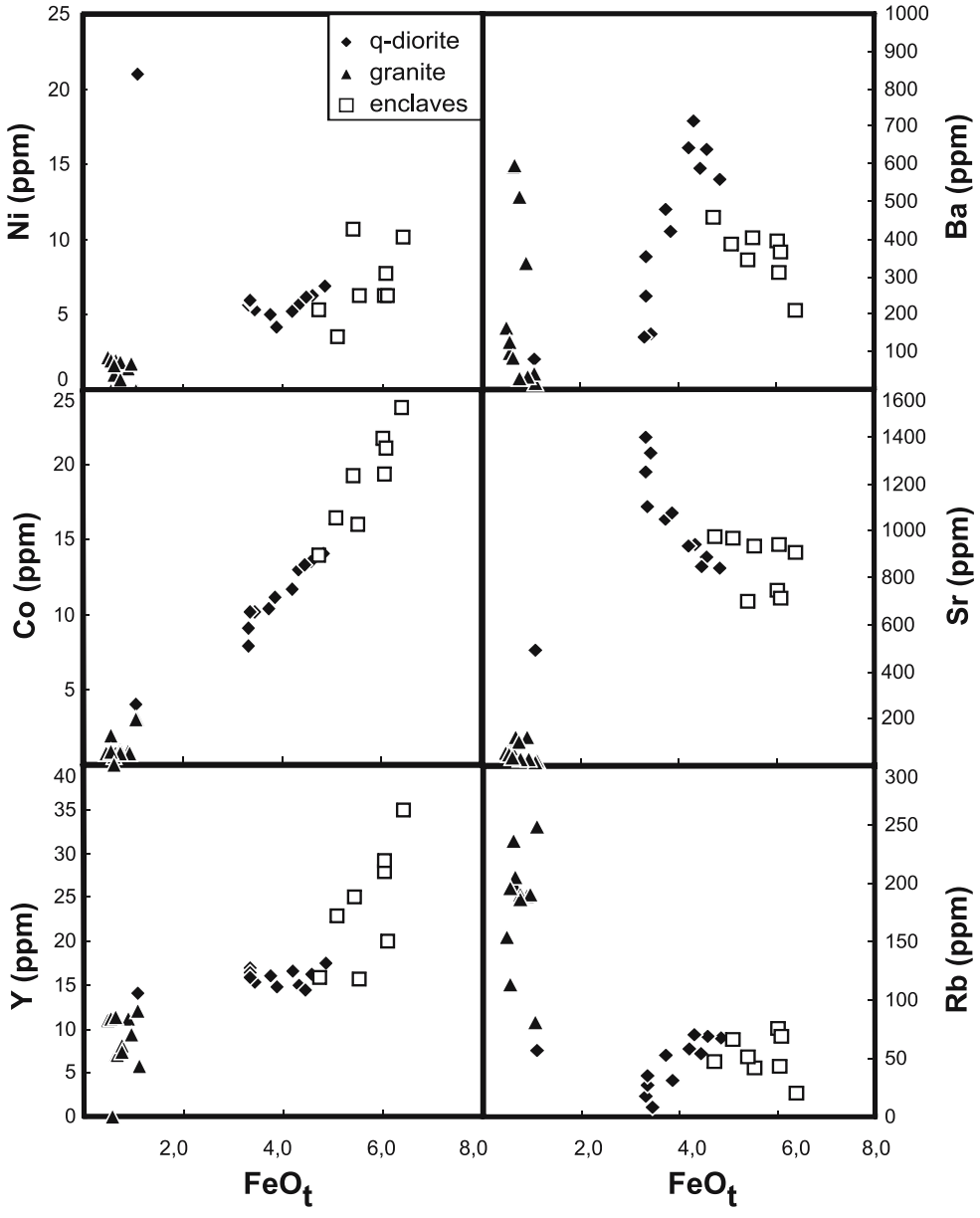

Fig. 15 FeO_t versus some trace elements variation plots for host rock, enclave, and granite samples

melting of the lower crust rocks with intermediate compositions and subsequent production of granitic melts. Mafic magma might melt surrounding crustal rocks in the lower crust only if it was trapped long enough to permit thermal exchange (Marsh 1982; Huppert and Sparks 1988; Annen and Sparks 2002). Thus, mafic magma that was injected into an open system in which granitoid magma was already moving upward did not have enough time to thoroughly mix with the felsic host and was disrupted into small-scattered blobs in the moving granitoid magma. Therefore, extensive interaction between the crustal and successive pulses of mantle-derived melts through mixing produced hybrid quartz diorite magma at depth. During ascent and emplacement, mingling continued and interaction between granitoid and MME involved thermal, mineral, and chemical transfers. Thermal diffusion is 100 times more rapid than chemical diffusion; therefore primarily hotter, more mafic magma batches can attain thermal equilibrium with felsic host magma prior to chemical equilibrium being reached (e.g., Sparks and Marshall 1986; Frost and Mahood 1987; Fernandez and Barbarin 1991). The rate of chemical transfer depends on the chemical contrast, the physical state of both components, and dynamics of the system (e.g., Cruden et al. 1995; Snyder and Tait 1995, 1998; Cardoso and Woods 1999; Tepper and Kuehner 2004).

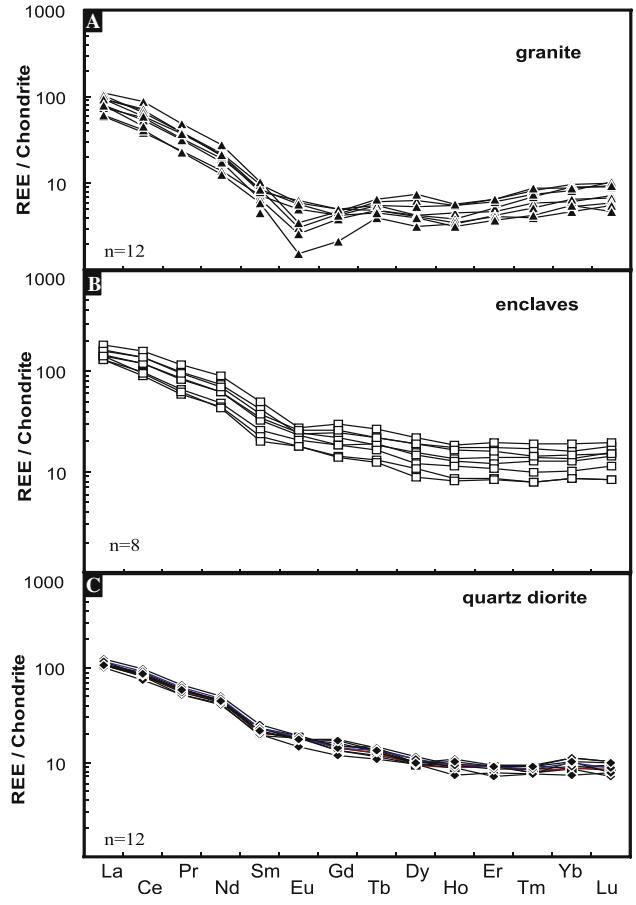

Fig. 16 Chondrite-normalized rare earth element patterns of quartz diorite, granite, and enclave samples. Normalizing values are from Boynton (1984)

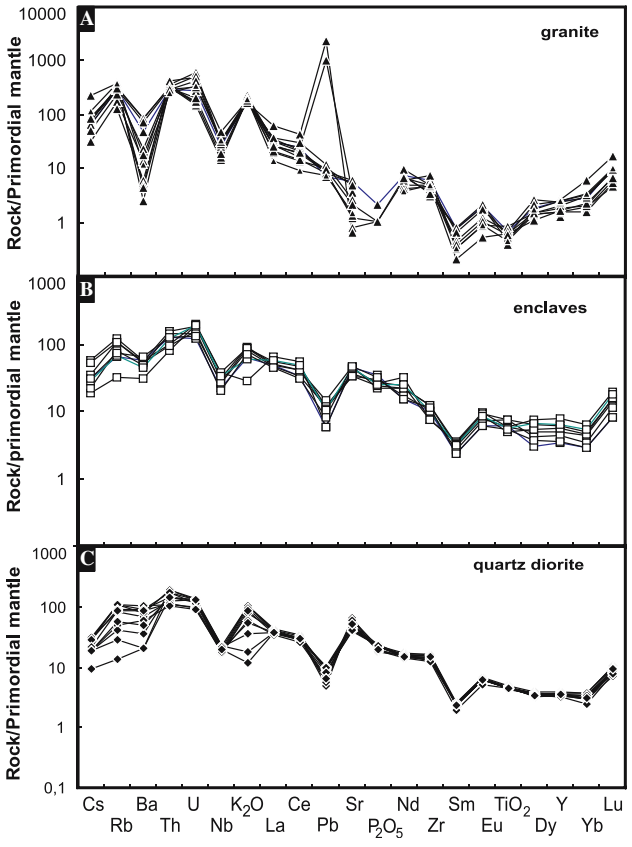

Fig. 17 Primitive mantle-normalized spider diagrams of quartz diorite, granite, and enclave samples. Normalizing values are from Sun and McDonough (1989)

Consequently, hybridization processes involving the Karamadazı Granitoid could have operated at two distinct but continuous periods and at different levels in the crust: (1) thorough mixing at depth-formed homogeneous magmas that crystallized to quartz diorites, probably with some MME; (2) mingling and local mixing during ascent and emplacement produced MME. The Karamadazı Granitoid thus may represent uniform hybrid rocks in which the two original mafic and felsic components are unknown. Sr and Nd isotopic data indicate that Central Anatolian calc-alkaline granitoid magmas were initially hybrids, produced from an enriched mantle source to which a subduction component had been added, or coupled crustal contamination with fractional crystallization, or both (Kadioglu et al. 2003; Ilbeyli et al. 2004).

Conclusions

The Karamadazı Granitoid is composed predominantly of granites and quartz diorites with MME displaying mineralogical and geochemical characteristics of I-type granitoids.

MME have xenocrysts with disequilibrium features indicating hybridization of mafic and felsic magmas: (1) plagioclases are embayed, and have heterogeneous

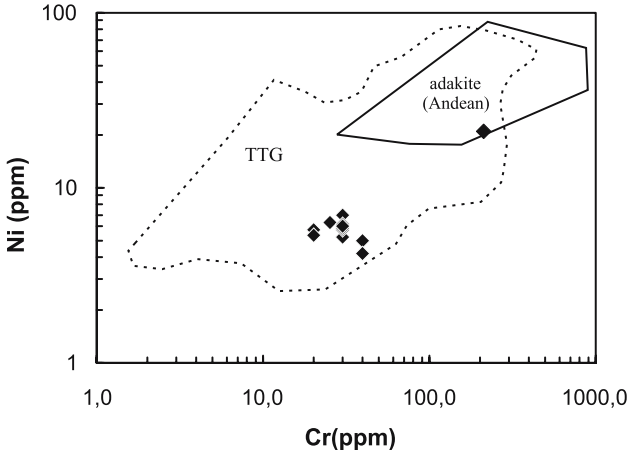

Fig. 18 Cr versus Ni variation plots for quartz diorites. Boundaries of tonalites–trondhjemites–granodiorites (*TTGs*) and adakite fields are from Condie (2005)

Table 7 Major (wt%), trace, and rare earth element (ppm) analyses of the Karamadazı Granitoid samples

	Quartz diorite					Enclaves					Granite				
Sample no.	49-1	40	38	36	45	35 E	36 E	37 E	40 E	74e	56	58	78	53	68
SiO_2	60.5	61.3	61.7	62.5	63.0	59.61	54.47	57.67	55.15	56.21	74.6	76.2	76.29	76.78	77.68
TiO_2	0.6	0.6	0.6	0.6	0.6	0.8	0.77	0.75	0.98	0.73	0.1	0.1	0.07	0.08	0.06
Al_2O_3	16.7	16.9	16.7	17.0	17.2	17.33	16.39	16.78	18.04	16.59	14.0	13.3	13.35	12.53	12.2
Fe_2O_3*	4.2	4.8	5.0	3.7	3.7	6.15	7.11	5.66	6.77	6.72	1.0	0.7	0.74	0.85	0.69
MgO	2.9	2.7	2.8	2.7	2.7	2.52	5.53	3.68	4.09	4.71	0.1	0.1	0.07	0.07	0.07
MnO	0.1	0.1	0.1	0.1	0.1	0.07	0.11	0.09	0.09	0.1	0.0	0.0	0.01	0.01	0.02
CaO	5.6	5.5	5.7	5.0	5.1	5.42	8.04	6.06	7.32	7.03	1.1	0.7	0.75	0.61	0.55
Na_2O	5.0	4.2	4.2	6.1	5.1	4.79	4.65	4.83	4.15	4.77	3.8	3.4	3.5	3.47	3.24
K_2O	2.0	2.5	2.2	0.4	1.3	1.52	0.7	2.3	2.02	1.5	4.6	4.9	4.89	4.57	4.92
P_2O_5	0.2	0.2	0.2	0.2	0.2	0.33	0.25	0.21	0.28	0.24	0.0	< .01	< .01	< .01	< .01
LOI	2.2	0.9	0.7	1.4	1.0	1.3	1.2	1.7	0.8	1.51	0.6	0.4	0.3	0.9	0.5
Total	99.8	99.6	99.8	99.7	100.0	99.8	99.2	99.7	99.7	100	99.8	99.8	99.97	99.87	99.93
Cr	40	20	30	30	30	< 10	190	20	< 10	60	< 10	< 10	< 10	< 10	< 10
Ni	5	6	6	6	6	6	10	4	6	8	2	1	2	1	2
Co	10	13	13	8	10	16	24	17	21	19	1	1	1	1	< .5
Sc	12	11	11	11	11	9	24	19	21	23	2	2	2	2	2
Cu	5	5	5	11	7	11	8	82	14	8	1	1	1	1	3
Ga	16	18	17	17	17	18	19	20	19	19	15	13	14	15	14
W	1	1	1	1	1	1	0	1	1	1	0	0	0	2	0
Pb	2	2	2	1	1	1	1	3	2	2	1	2	2	2	1
Zn	14	17	26	11	16	17	11	14	17	12	7	3	4	3	5
Cs	1	1	1	1	1	1	1	1	2	1	2	2	3	2	4
Rb	53	70	54	18	36	41	21	67	69	44	189	198	206	186	237
Sr	1046	939	848	1395	1102	933	908	969	711	942	123	114	124	29	32
Ba	479	715	588	140	352	402	212	385	367	310	337	592	598	31	84
Zr	147	157	156	180	169	114	85	135	116	110	68	38	40	51	55
Hf	4	4	5	5	5	3	3	4	3	3	3	2	2	2	3
Nb	12	14	12	16	14	15	27	22	19	23	19	11	11	23	24
Ta	1	1	1	1	1	1	2	2	1	2	3	1	2	3	2
Th	11	9	10	16	12	11	7	13	8	10	25	28	27	25	21
U	3	2	2	3	3	3	4	4	3	4	6	3	4	7	7
Y	16	15	15	17	16	16	35	23	20	29	11	7	7	7	11
La	27.7	26.5	25.1	25.9	25.6	33.7	43.9	34.7	31.3	39.1	21.9	21.9	24.1	14.3	9.5
Ce	51.5	52.2	49.7	54.3	52.1	58	98.3	72.6	59.5	85.2	42.3	36.5	39.9	25.2	16.2
Pr	5.6	5.4	5.0	5.7	5.3	5.86	11.14	7.89	6.19	9.23	3.7	3.5	3.63	2.18	1.51
Nd	21.3	20.7	19.5	21.2	20.4	20.2	42.5	29.5	22.9	34.4	10.2	10.0	9.5	5.8	5.2
Sm	3.5	3.1	2.9	3.5	3.2	3.1	7.6	5	4	6.4	1.5	1.3	1.2	0.9	1
Eu	1.1	1.1	1.0	1.0	1.0	1.04	1.6	1.33	1.2	1.4	0.3	0.3	0.36	0.09	0.15
Gd	3.1	2.8	2.8	3.6	3.3	2.83	6.16	3.79	3.8	5.02	1.0	0.9	1.04	0.44	0.81
Tb	0.5	0.5	0.4	0.5	0.5	0.47	0.99	0.71	0.61	0.82	0.2	0.2	0.18	0.15	0.22
Dy	2.7	2.6	2.4	2.5	2.5	2.23	5.59	3.7	3.09	4.8	1.4	1.0	1.04	0.8	1.28
Ho	0.5	0.5	0.4	0.6	0.5	0.46	1.04	0.72	0.65	0.98	0.3	0.2	0.2	0.19	0.3
Er	1.6	1.5	1.3	1.6	1.4	1.39	3.24	2.01	1.78	2.9	1.0	0.6	0.68	0.7	1.11
Tm	0.2	0.2	0.2	0.2	0.2	0.2	0.48	0.33	0.25	0.43	0.2	0.1	0.1	0.13	0.2
Yb	1.4	1.4	1.2	1.9	1.5	1.42	3.18	2.12	1.68	2.64	1.4	0.9	0.79	1.1	1.72
Lu	0.2	0.2	0.2	0.3	0.2	0.21	0.5	0.36	0.29	0.45	0.3	0.1	0.14	0.17	0.26
Na_2O+K_2O	7.0	6.8	6.4	6.6	6.4	6.31	5.35	7.13	6.17	6.27	8.3	8.4	8.39	8.04	8.16
A/CNK	1.08	1.16	1.16	1.12	1.19	1.19	1.04	1.05	1.15	1.05	1.2	1.1	1.14	1.12	1.09
Mg#	58	52	53	59	59	45	61	56	55	58	21	14	16	14	17

Fe_2O_3* is total iron as Fe_2O_3 and LOI is loss on ignition

Mg#: molar $100 \times (Mg/Mg + Fe^{2+})$

core and rim compositions; (2) plagioclase crystals have reverse, normal, and oscillatory zoning. (3) hornblende and augite crystals have normal and inverse chemical zoning in terms of $Mg/(Mg+Fe^{2+})$ ratio.

From the combined textural, geochemical whole-rock, and chemical mineral data presented herein, there is concurrent evidence to support a magmatic origin for the common MME occurring in the Karamadazı Granitoid; they are interpreted as products of

arrested hybridization of mantle-derived mafic magma that mingled with partly crystallized quartz diorites magma. Quartz diorites are high-Al TTG in origin, and are suggested to be formed by mixing of granitoid produced by partial melting of lower crust, with MME magma. The leucogranites have geochemical characteristics distinct from the quartz diorites and their enclaves, and are suggested to be not involved in producing MME.

Acknowledgements This work was financially supported by the Office of Scientific Research at Selcuk University, Konya-Turkey (Bu calısma Selcuk Universitesi Bilimsel Arastırma projeleri tarafından desteklenmistir. BAP; Project number: 2004-047). A.P. Boyle and E.C. Ferré are gratefully acknowledged for their critical reviews resulting in substantial improvement of an early draft. Special thanks also to M. Arslan for critical comments on the manuscript.

References

Akiman O, Erler A, Goncuoglu MC, Gulec N, Geven A, Tureli TK, Kadioglu YK (1993) Geochemical characteristics of granitoids along the western margin of the Central Anatolian Crystalline Complex and their tectonic implications. Geol J 28:371–382

Annen C, Sparks RSJ (2002) Effects of repetitive emplacement of basaltic intrusions on thermal evolution and melt generation in the crust. Earth Planet Sci Lett 203:937–955

Aydin N, Goncuoglu MC, Erler A (1998) Latest Cretaceous magmatism in the Central Anatolian Crystalline Complex: brief review of field, petrographic and geochemical features. Turk J Earth Sci 7:259–268

Barbarin B (2005) Mafic magmatic enclaves and mafic rocks associated with some granitoids of the central Sierra Nevada batholith, California: nature, origin, and relations with the hosts. Lithos 80:155–177

Barbarin B, Didier J (1992) Genesis and evolution of mafic microgranular enclaves through various types of interaction between coexisting felsic and mafic magmas. Trans R Soc Edin: Earth Sci 83:145–153

Bloomfield AL, Arculus RJ (1989) Magma mixing in the San Francisco Volcanic Field, AZ. Contrib. Mineral Petrol 102:429–453

Blundy JD, Sparks RSJ (1992) Petrogenesis of mafic inclusions in granitoids of the Adamello Massif, Italy. J Petrol 33:1039–1104

Boynton WV (1984) Cosmochemistry of the rare earth elements: meteorite studies. In: Henderson P (ed) Rare earth elements. Elsevier, pp 63–114

Boztug D (1998) Post-collisional central Anatolian alkaline plutonism, Turkey. Turk Earth Sci 7:145–165

Boztug D (2000) S-I-A intrusive associations: geodynamic significance of synchronism between metamorphism and magmatism in Central Anatolia, Turkey. In: Bozkurt E, Winchester JA, Piper JDA (eds) Geol Soc Lond Spec Publ 173:441–458

Boztug D, Cevikbas A, Demirkol C, Tatar S, Akyıldız M, Otlu N (2002) Mineralogical–petrographical and geochemical study of the Karamadazi pluton, Yahyalt-Kayseri, Central Anatolia, Turkey. Geol Bull Turkey 45/1:41–58

Cardoso SS, Woods AW (1999) On convection in a volatile-saturated magma. Earth Planet Sci Lett 168/3–4: 301–310

Chappel BW, White AJR (1974) Two contrasting granite types. Pac Geo 8:173–174

Chappel BW, White AJR (1992) I- and S-types granites in the Lachland Fold Belt. Trans Royal Soc Edin: Earth Sci 83:1–26

Chappell BW, White AJR, Wyborn D (1987) The importance of residual source material restite in granite petrogenesis. J Petrol 28:1111–1138

Chen YD, Price RC, White AJR, Chappell BW (1989) Inclusions in three S-type granites from southeastern Australia. J Petrol 30:1181–1218

Condie KC (2005) TTGs and adakites: are they both slab melts? Lithos 80:33– 44

Cruden AR, Koyi H, Schmelinget H (1995) Diapiric basal entrainment of mafic into felsic magma. Earth Planetary Sci Lett 131/3–4:321–340

Dahlquist JA (2002) Mafic microgranular enclaves: early segregation from metaluminous magma (Sierra de Chepes), Pampean Ranges, NW Argentina. J S Am Earth Sci 15/6: 643–655

Debon F, Le Fort P (1982) A chemical–mineralogical classification of common plutonic rocks and associations. TRSE Earth Sci 73:135–149

Defant MJ, Drummond MS (1990) Derivation of some modern arc magmas by melting of young subducted lithosphere. Nature 347:662–665

Defant MJ, Drummond MS (1993) Mount St. Helens: potential example of the partial melting of the subducted lithosphere in a volcanic arc. Geology 21:547–550

Didier J (1973) Granites and their enclaves. Elsevier, London, p 393

Didier J, Barbarin B (1991) Enclaves and granite petrology. Developments in petrology, vol 13. Elsevier, Amsterdam

Dilek Y, Whitney DL, Tekeli O (1999) Links between tectonic processes and landscape morphology in an Alpine collision zone, South-Central Turkey. Zeitschrift Geomorphologie NF 118:147–164

Dodge FCW, Kistler RW (1990) Some additional observations on inclusions in the granitic rocks of the Sierra Nevada. J Geophys Res 95:17841–17848

Droop GTR (1987) A general equation for estimating Fe^{3+} concentrations in ferromagnesian silicates and oxides from microprobe analyses, using stochiometric criteria. Mineral Mag 51:431–435

Elburg MA (1996) Evidence of isotopic equilibration between microgranitoid enclaves and host granodiorite. Warburton Granodiorite, Lachlan Fold Belt, Australia. Lithos 38:1–22

Erler A, Goncuoglu MC (1996) Geologic and tectonic setting of the Yozgat Batholith, northern Central Anatolian Crystalline Complex, Turkey. Int Geo Rev 38:714–726

Fernandez AN, Barbarin B (1991) Relative rheology of coeval mafic and felsic magmas: nature of resulting interaction processes and shape and mineral fabrics of mafic microgranular enclaves. In: Didier J, Barbarin B (eds) Enclaves and granite petrology, developments in petrology. Elsevier, Amsterdam, pp 263–275

Frost TP, Mahood GA (1987) Field, chemical, and physical constraints on mafic–felsic magma interaction in the Lamarck Granodiorite, Sierra Nevada, California. Geol Soc Am Bull 99:272–291

Goncuoglu MC, Tureli K (1994) Alpine collisional-type granitoids from western Central Anatolian Crystalline Complex, Turkey. J Kocaeli Univ, Earth Sci Sect 1:39–46

Goncuoglu MC, Toprak V, Kuscu U, Erler A, Olgun E (1991) Geology of the Western part of the Central Anatolian Massif, Part 1: Southern Part. Turkish Petroleum Corporation (TPAO) Project Report No. 2909 (in Turkish, unpublished)

Goncuoglu MC, Erler A, Toprak GMV, Olgun E, Yalınız K, Kuscu İ, Koksal S, Dirik K (1993) Orta Anadolu Masifi'nin orta bolumunun jeolojisi, Bolum 3: Orta Kızılırmak Tersiyer baseninin jeolojik evrimi. TPAO Rep. No. 3313 (p 104, in Turkish)

Gorur N, Oktay F, Seymen İ, Sengor AMC (1984) Paleotectonic evolution of the Tuzgolu basin complex, central Turkey: sedimentary record of a Neo-Tethyan closure In: Dixon JE, Robertson AHF (eds) The geological evolution of the Eastern Mediterranean geological society, London, Special Publications 17:467–482

Gorur N, Tuysuz O, Sengor AMC (1998) Tectonic evolution of the Central Anatolian basins. Int Geo Rev 40:831–850

Hofmann A, Jochum K, Seufert M, White M (1986) Nb and Pb in oceanic basalts: New constraints on mantle evolution. Earth Planet Sci Lett 33:33–45

Holden P, Halliday AN, Stepens WE (1987) Neodymium and strontium isotope content of microdiorite enclaves points to mantle input to granitoid production. Nature 330:53–56

Huppert HE, Sparks RSJ (1988) The generation of granitic magmas by intrusion of basalt into continental crust. J Petrol 29:599–624

Ilbeyli N, Pearce JA, Thirlwall MF, Mitchell JG (2004) Petrogenesis of collision-related plutonics in Central Anatolia, Turkey. Lithos 72:3–4, 163–182

Johnston AD, Wyllie PJ (1988) Interaction of granitic and basic magmas: experimental observations on contamination processes at 10 kbar with H_2O. Contribu Mineral Petrol 98:352–362

Kadioglu YK, Gulec N (1996) Mafic microgranular enclaves and interaction between felsic and mafic magmas in the Agacoren intrusive suite: evidence for petrographic features and mineral chemistry. Int Geol Rev 38:854–867

Kadioglu YK, Dilek Y, Gulec N, Foland KA (2003) Tectonomagmatic evolution of bimodal plutons in the Central Anatolian Crystalline Complex, Turkey. J Geo 11:671–690

Klein M, Stosch HG, Seck HA (1997) Partitioning of high field-strength and rare-earth elements between amphibole, and quartz dioritic to tonalitic melts: an experimental study. Chem Geol 138:257–271

Kocak K (1993) The petrology and geochemistry of the Ortakoy area, Central Turkey: PhD thesis, Glasgow Univ, Scotland, p 280 (unpublished)

Kocak K, Leake BE (1994) The petrology of the Ortakoy district and its ophiolite at the western edge of the Middle Anatolian Massif, Turkey. J A Earth Sci 18/2:163–174

Kuscu GG, Goncuoglu MC, Kuscu I (2001) Post-collisional magmatism on the northern margin of the Taurides and its geological implications: geology and petrology of the Yahyalı-Karamadazı Granitoid. TJES (Turkish) 10:103–119

Lameyre J, Bonin B (1991) Granites in the main plutonic series. In: Didier J, Barbarin B (eds) Enclaves and granite petrology. Elsevier, Amsterdam, pp 3–17

Le Maitre RW, Bateman P, Dudek A, Keller J, Lameyre Le Bas MJ, Sabine PA, Schmid R, Sorensen H, Streckeisen A, Woolley AR, Zanettin B (1989) A classification of igneous rocks and glossary of terms. Blackwell, Oxford

Leake BE, Woolley AR, Arps CES, Birch WD, Gilbert MC, Grice JD, Hawthorne FC, Kato A, Kisch HJ, Krivovichev VG, Linthout K, Laird J, Mandarino JA, Maresch WV, Nickel EH, Rock NMS, Schumacher JC, Smith DC, Stephenson NCN, Ungaretti L, Whittaker EJW, Youzhi G (1997) Nomenclature of amphiboles: report of the subcomittee on amphiboles of the international mineralogical association, commission on new minerals and mineral names. Am Mineral 82:1019–1037

López-Moro FJ (2000) Las Rocas Plutónicas Calcoalcalinas y Shoshoníticas del Domo Varisco del Tormes (Centro-Oeste Espanol). Estudio mineralógico, geoquímico y petrogenético. PhD Thesis, Univ. Salamanca, Spain

López-Ruíz J, Cebriá JM (1990) Geoquímica de los Processos Magmáticos. Rueda, Madrid

Maas R, Nicholls IA, Legg C (1997) Igneous and metamorphic enclaves in the S-type Deddick Granodiorite, Lachlan Fold Belt SE Australia: petrographic, geochemical and Nd–Sr isotopic evidence for crustal melting and magma mixing. J Petrol 38:815–841

Marsh BD (1982) On the mechanics of igneous diapirism, stoping, and zone melting. Am J Sci 282:808– 855

Michael PJ (1991) Intrusion of basaltic magma into a crystallizing granitic magma chamber: the Cordillera del Paine pluton in southern Chile. Contrib Mineral Petrol 108:396–418

Morimoto N (1988) Nomenclature of pyroxenes. Mineral Mag 52:535–550

Nachit H, Razafimahefa N, Stussi JM, Carron JP (1985) Composition chimique des biotites et typologie magmatique des granitoides. Comptes Rendus de l'Academie des Sciences' de Paris 301:813–818

Oygur V (1986) Geology and formation of the Karamadazı (Yahyalı-Kayseri) contact metasomatic magnetite deposit. Jeoloji Muhendisligi 27:1–9 [in Turkish with English abstract]

Oygur V, Yurt MZ, Yurt F, Sarı U (1978) Geological report on the Kayseri-Yahyalı- Karamadazı and Kovalı iron-ore deposits. General Directorate of Mineral Research and Exploration (MTA) Report No. 6609 (in Turkish, unpublished)

Parada MA, Nystrom JO, Levi B (1999) Multiple sources for the Coastal Batholith of central Chile (31–34 S): geochemical and Sr–Nd isotopic evidence and tectonic implications. Lithos 46:505–521

Pearce JA (1983) Role of the sub-continental lithosphere in magma genesis at active continental margins. In: Hawkesworth CJ (ed) Continental basalts and mantle xenoliths. Shiva, Nantwich, pp 230–249

Peccerillo A, Taylor SR (1976) Geochemistry of Eocene calcalkaline volcanic rocks from the Kastamonu area, northern Turkey. Contrib Mineral Petrol 58:63–81

Pitcher WS (1991) Synplutonic dykes and mafic enclaves. In: Didier J, Barbarin B (eds) Enclaves and granite petrology. Dev Petrol, Amsterdam, Elsevier, pp 383–391

Prouteau G, Scaillet B, Pichavant M, Maury RC (2001) Evidence for mantle metasomatism by hydrous silicic melts derived from subducted oceanic crust. Nature 410:197–200

Rapp RP, Watson EB, Miller CF (1991) Partial melting of amphibolite eclogite and the origin of Archean trondhjemites and tonalites. Precambrian Res 51:1–25

Romick JD, Kay SM, Kay RM (1992) The influence of amphibole fractionation on the evolution of calc-alkaline andesite and dacite tehpra from the central Aleutians, Alaska. Contrib Mineral Petrol 112:101–118

Rudnick RL, Fountain DM (1995) Nature and composition of the continental crust: a lower crustal perspective. Rev Geophys 33:267–309

Rushmer T (1990) Partial melting of two amphibolites: contrasting experimental results under fluid-absent conditions. Contrib Mineral Petrol 107:41–59

Rutter MJ, Wyllie PJ (1988) Melting of vapour-absent tonalite at 10 kbar to simulate dehydration melting in the deep crust. Nature 331:159–160

Şengör AMC, Yilmaz Y (1981) Tethyan evolution of Turkey: a plate tectonic approach. Tectonophysics 75:181–241

Shaw A, Downes H, Thirwall MF (1993) The quartz-diorites of Limousin: elemental and isotopic evidence for Devono-Carboniferous subduction in the Hercynian belt of the French Massif Central. Chem Geol 107:1–18

Silva MMVG, Neiva AMR, Whitehouse MJ (2000) Geochemistry of enclaves and host granites from the Nelas area, central Portugal. Lithos 50:153–170

Smithies RH (2000) The Archaean tonalite–trondhjemite–granodiorite (TTG) series is not an analogue of Cenozoic adakite. Earth Planet Sci Lett 182:115–125

Snyder D, Tait S (1995) Replenishment of magma chambers: comparison of fluid-mechanic experiments with field relations Contrib. Mineral. Petrol 122: 230–240

Snyder D, Tait SR (1998) The imprint of basalt on the geochemistry of silicic magmas. Earth Planetary Sci Lett 160:433–445

Sparks RSJ, Marshall LA (1986) Thermal and mechanical constraints on mixing between mafic and silicic magmas. J Volcanol Geotherm Res 29:99–124

Stamatelopoulou-Seymour K, Vlassopoulos D, Pearce TH, Rice C (1990) The record of magma chamber processes in plagioclase phenocrysts at Thera Volcano, Aegean Volcanic Arc, Greece. Contrib Mineral Petrol 104:73–84

Stimac JA, Pearce TH (1992) Textural evidence of mafic–felsic magma interaction in dacite lavas, Clear Lake, California. Am Mineral 77:795–809

Sun SS, McDonough WF (1989) Chemical and isotopic systematics of oceanic basalts: implications for mantle composition and processes. In: Saunders AD, Norry MJ (eds) Magmatism in the ocean basins. Geo Soc Spec Pub 42:313–345

Tepper JH, Kuehner SM (2004) Geochemistry of mafic enclaves and host granitoids from the Chilliwack Batholith, Washington: chemical exchange processes between coexisting mafic and felsic magmas and implications for the interpretation of enclave chemical traits. J Geol 112:349–367

Vernon RH (1983) Restite, xenoliths and microgranitoid enclaves in granites. J Proc R Soc N S W 116:77–103

Vernon RH (1990) Crystallization and hybridism in microgranitoid enclave magmas: microstructural evidence. J Geophys Res 95:17849–17859

White RV, Tarney J, Kerr AC, Saunders AD, Kempton PD, Pringle MS, Klaver GT (1999) Modification of an oceanic plateau, Aruba, Dutch Caribbean: implications for the generation of continental crust. Lithos 46:43–68

Wyllie PJ, Cox KG, Biggar GM (1962) The habit of apatite in synthetic systems and igneous rocks. J Petrol 3:238–243

Yaliniz MK, Aydin NS, Goncuoglu MC, Parlak O (1999) Terlemez quartz monzonite of Central Anatolia (Aksaray-Sarikaraman): age, petrogenesis and geotectonic implications for ophiolite emplacement. Geol J 34:233–242